



HAL
open science

The Dynamics of CO₂-Driven Granular Flows in Gullies on Mars

Lonneke Roelofs, Susan J Conway, Bas van Dam, Arjan van Eijk, Jonathan P Merrison, Jens Jacob Iversen, Matthew Sylvest, Manish R Patel, Henk Markies, Marcel van Maarseveen, et al.

► **To cite this version:**

Lonneke Roelofs, Susan J Conway, Bas van Dam, Arjan van Eijk, Jonathan P Merrison, et al.. The Dynamics of CO₂-Driven Granular Flows in Gullies on Mars. *Journal of Geophysical Research. Planets*, 2024, 129 (6), 10.1029/2024JE008319. hal-04667675

HAL Id: hal-04667675

<https://hal.science/hal-04667675v1>

Submitted on 5 Aug 2024

HAL is a multi-disciplinary open access archive for the deposit and dissemination of scientific research documents, whether they are published or not. The documents may come from teaching and research institutions in France or abroad, or from public or private research centers.

L'archive ouverte pluridisciplinaire **HAL**, est destinée au dépôt et à la diffusion de documents scientifiques de niveau recherche, publiés ou non, émanant des établissements d'enseignement et de recherche français ou étrangers, des laboratoires publics ou privés.

The Dynamics of CO₂-Driven Granular Flows in Gullies on Mars

**Key Points:**

- The sublimation of small amounts of CO₂ ice can fluidize granular material on low slopes under Martian atmospheric pressure
- The flow dynamics of CO₂-driven flows are similar to that of terrestrial fluidized two-phase flows, for example, debris flows and dense pyroclastic flows
- Experimental CO₂-driven granular flows create deposit morphologies similar to those observed in Martian gullies

Supporting Information:

Supporting Information may be found in the online version of this article.

Correspondence to:

L. Roelofs,
l.roelofs@uu.nl

Citation:








Roelofs, L., Conway, S. J., van Dam, B., van Eijk, A., Merrison, J. P., Iversen, J. J., et al. (2024). The dynamics of CO₂-driven granular flows in gullies on Mars. *Journal of Geophysical Research: Planets*, 129, e2024JE008319. <https://doi.org/10.1029/2024JE008319>

Received 6 FEB 2024

Accepted 7 MAY 2024

Author Contributions:

Conceptualization: Lonneke Roelofs, Susan J. Conway, Susan J. Conway
Data curation: Lonneke Roelofs
Formal analysis: Lonneke Roelofs, Susan J. Conway, Jonathan P. Merrison, Jim McElwaine, Maarten G. Kleinhans, Maarten G. Kleinhans
Funding acquisition: Lonneke Roelofs, Susan J. Conway, Jonathan P. Merrison, Manish R. Patel, Manish R. Patel
Investigation: Lonneke Roelofs, Lonneke Roelofs, Jonathan P. Merrison, Jens Jacob Iversen, Matthew Sylvest
Methodology: Lonneke Roelofs, Susan J. Conway, Susan J. Conway, Susan J. Conway, Jonathan P. Merrison, Jens

Lonneke Roelofs¹ , Susan J. Conway² , Bas van Dam¹, Arjan van Eijk¹, Jonathan P. Merrison³, Jens Jacob Iversen³, Matthew Sylvest⁴ , Manish R. Patel⁴ , Henk Markies¹, Marcel van Maarseveen¹, Jim McElwaine⁵ , Maarten G. Kleinhans¹ , and Tjalling de Haas¹ 

¹Department of Physical Geography, Faculty of Geosciences, Utrecht University, Utrecht, The Netherlands, ²Laboratoire de Planétologie et Géosciences, Nantes Université, University Angers, Le Mans Université, CNRS, LPG UMR 6112, Nantes, France, ³Mars Simulation Laboratory, Aarhus University, Århus, Denmark, ⁴School of Physical Sciences, The Open University, Milton Keynes, UK, ⁵Department of Earth Sciences, Durham University, Durham, UK

Abstract Martian gullies are landforms consisting of an erosional alcove, a channel, and a depositional apron. A significant proportion of Martian gullies at the mid-latitudes is active today. The seasonal sublimation of CO₂ ice has been suggested as a driver behind present-day gully activity. However, due to a lack of in situ observations, the actual processes causing the observed changes remain unresolved. Here, we present results from flume experiments in environmental chambers in which we created CO₂-driven granular flows under Martian atmospheric conditions. Our experiments show that under Martian atmospheric pressure, large amounts of granular material can be fluidized by the sublimation of small quantities of CO₂ ice in the granular mixture (only 0.5% of the volume fraction of the flow) under slope angles as low as 10°. Dimensionless scaling of the CO₂-driven granular flows shows that they are dynamically similar to terrestrial two-phase granular flows, that is, debris flows and pyroclastic flows. The similarity in flow dynamics explains the similarity in deposit morphology with levees and lobes, supporting the hypothesis that CO₂-driven granular flows on Mars are not merely modifying older landforms, but they are actively forming them. This has far-reaching implications for the processes thought to have formed these gullies over time. For other planetary bodies in our solar system, our experimental results suggest that the existence of gully like landforms is not necessarily evidence for flowing liquids but that they could also be formed or modified by sublimation-driven flow processes.

Plain Language Summary Gullies on Mars are features that look like landforms carved by debris flows on Earth. At the top, the gullies have an erosional alcove where material is eroded and at the bottom of the gully, a fan exists where this material is deposited. For a long time, it was believed that these gullies were formed by liquid water, just like on Earth. However, Martian gullies are active today, which cannot be reconciled with the lack of liquid water on the surface of Mars. Data from satellites has shown that the activity in Martian gullies is correlated to a seasonal cycle of CO₂ ice deposition and sublimation. However, we still do not know whether and how CO₂ sublimation produces the observed changes in gullies. Here we show the results of experiments in environmental chambers in which we created CO₂-driven flows under Martian conditions. The experiments show that granular material can be fluidized by sublimation of CO₂ ice. Furthermore, the flow dynamics and morphology of the deposits are similar to debris flows and pyroclastic flows on Earth. This explains the similarity between the Martian gullies and the water-shaped gullies on Earth without the presence of liquid water on the surface of Mars today.

1. Introduction

Despite the lack of stable liquid water on Mars today (Hecht, 2002; Richardson & Mischna, 2005), Mars is a geomorphologically active planet. Numerous studies in the last decades have documented a range of geomorphic activities (for an overview see (Diniega et al., 2021)). Among the most active landforms on Mars are Martian gullies (Figure 1). These landforms consist of an erosional alcove, a channel, and a depositional apron and resemble debris flow systems on Earth (Conway et al., 2011; Costard et al., 2002; de Haas, Hauber, et al., 2015; Johnsson et al., 2014; Malin & Edgett, 2000). Since their discovery, Martian gullies have been a topic of scientific debate because of the possible link between their formation and liquid water (Costard et al., 2002; de Haas, Hauber, et al., 2015; Dickson et al., 2023; Malin & Edgett, 2000), and thus planetary habitability (Cottin et al., 2017; Hoffman, 2002).

© 2024. The Author(s).

This is an open access article under the terms of the [Creative Commons Attribution License](https://creativecommons.org/licenses/by/4.0/), which permits use, distribution and reproduction in any medium, provided the original work is properly cited.

Jacob Iversen, Matthew Sylvest,
Henk Markies, Henk Markies,
Henk Markies

Project administration:

Lonneke Roelofs, Lonneke Roelofs

Resources: Lonneke Roelofs,

Lonneke Roelofs, Jonathan P. Merrison,

Jens Jacob Iversen, Matthew Sylvest,

Manish R. Patel, Henk Markies,

Henk Markies

Software: Henk Markies

Supervision: Susan J. Conway, Maarten

G. Kleinhans, Maarten G. Kleinhans

Visualization: Lonneke Roelofs

Writing – original draft:

Lonneke Roelofs

Writing – review & editing:

Lonneke Roelofs, Susan J. Conway,

Jonathan P. Merrison, Matthew Sylvest,

Manish R. Patel, Jim McElwaine, Maarten

G. Kleinhans, Maarten G. Kleinhans

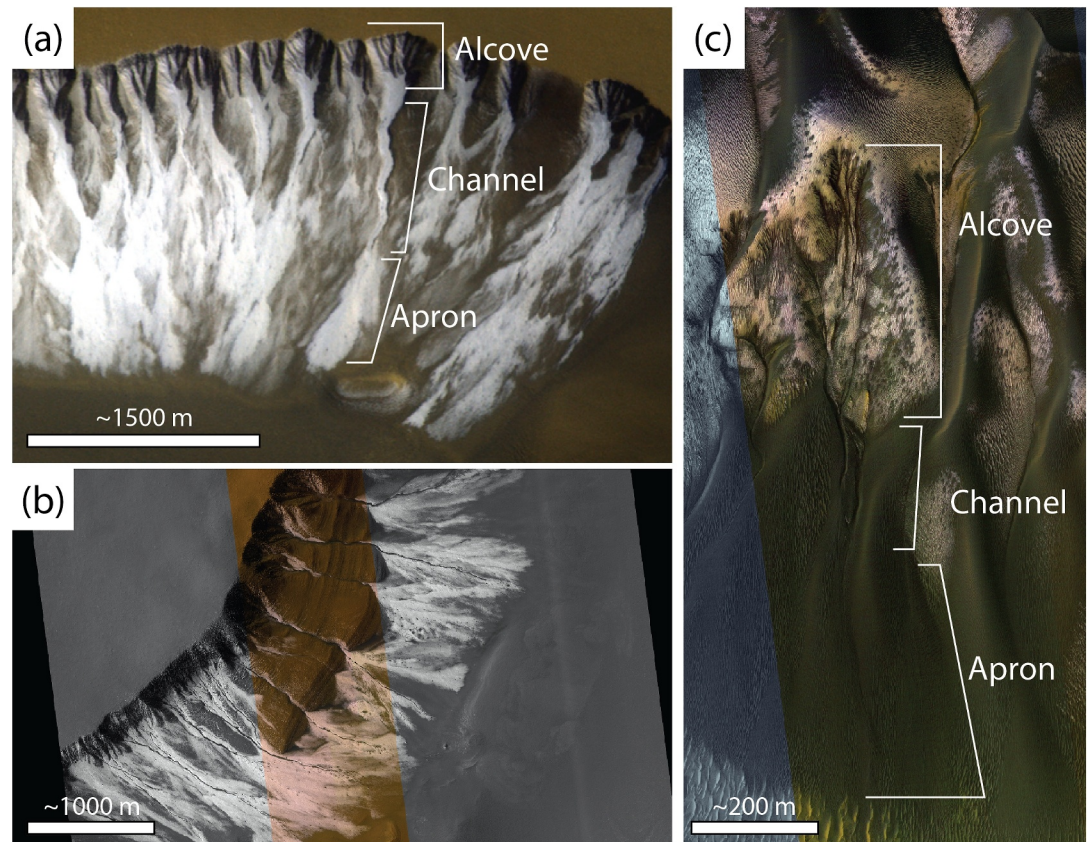


Figure 1. Three examples of Martian gullies with frost; (a) gullies in Sisyphi Cavi (synthetic RGB CaSSIS images using the PAN and BLU channels, where defrosted surfaces appear red and frosted surfaces white, MY34_003464_256_1, Ls 242°) (Pasquon et al., 2023), (b) gullies in an unnamed crater (HiRISE image, ESP_039114_1115, Ls 243°), (c) gullies on Matara crater dune field (HiRISE image, ESP_063824_1340, Ls 160°). Color strips in panels (b) and (c) are false colors, composed of near-infrared, red and blue-green wavelength signals.

Present-day activity in gullies is observed in subsequent images as new depositional lobes on aprons, the carving of new channels, and the movement of meter-scale boulders (Dinięga et al., 2010; Dundas et al., 2010, 2015; Raack et al., 2020; Sinha & Ray, 2023). As this activity is observed on slopes as low as 10° (Dundas et al., 2019), the material needs to have been fluidized to a certain degree (de Haas et al., 2019) and thus dry granular processes cannot have been the cause of the change. In the last decade, the leading hypothesis behind the recent activity in these gullies has shifted from water-driven flows (with or without the involvement of brines) (e.g., Conway et al., 2011; Costard et al., 2002; de Haas, Hauber, et al., 2015; Johnsson et al., 2014; Knauth & Burt, 2002; Lanza et al., 2010; Levy et al., 2010; Malin & Edgett, 2000) to flows driven by the sublimation of CO₂ frost (e.g., de Haas et al., 2019; Dinięga et al., 2010; Dundas et al., 2010, 2012, 2015, 2022; Khuller et al., 2021; Pasquon et al., 2023; Pilorget & Forget, 2016; Raack et al., 2015, 2020; Sinha & Ray, 2023). This shift is inspired by the lack of stable water on the Martian surface (Haberle et al., 2001; Hecht, 2002; Martinez et al., 2017; Richardson & Mischna, 2005) and a suite of remote sensing studies, showcasing the correlation between the spatial and temporal distribution of gully activity with that of CO₂ frost on the surface of Mars (Dinięga et al., 2010; Dundas et al., 2010, 2012, 2015, 2022; Khuller et al., 2021; Pasquon et al., 2019, 2023; Raack et al., 2015, 2020; Sinha & Ray, 2023) (e.g., see Figure 1). The CO₂-driven granular flow hypothesis is supported by modeling studies advocating for the possibility of CO₂ gas to fluidize granular material under the thin Martian atmosphere when CO₂ sublimates (Cedillo-Flores et al., 2011; de Haas et al., 2019; Pilorget & Forget, 2016). Furthermore, experimental studies have proven that the sublimation of CO₂ ice in the thin Martian atmosphere can destabilize granular materials on slopes (Sylvest et al., 2016, 2019) and even fluidize small volumes of granular material on low slope angles (Roelofs, Conway, de Haas, et al., 2024). The low atmospheric pressure of the Martian atmosphere is key in this process because of the large gas flux that is created when CO₂ ice sublimates and turns into

CO₂ gas (de Haas et al., 2019; Diniega et al., 2013; Roelofs, Conway, de Haas, et al., 2024; Sylvest et al., 2016, 2019). The gas flux, induced by the sublimation, depends on the ratio between the density of CO₂ ice and gas. In the thin Martian atmosphere (~800 Pa), the gas flux created by CO₂ sublimation is >100 larger than under Earth's atmosphere and thus likely sufficient to fluidize sediments (Cedillo-Flores et al., 2011; de Haas et al., 2019).

There are currently two “source-to-sink” hypotheses that attempt to explain how and why CO₂ ice sublimates near granular material on Mars, how this process mobilizes the granular material, and how it transports it over longer distances. The first hypothesis considers a layer of translucent CO₂ ice on top of a layer of regolith (Pilorget & Forget, 2016). This hypothesis is, in essence, the “Kieffer model,” explaining the formation of high-latitude defrosting spots (Kieffer, 2007), on a slope. According to this model, the translucency of CO₂ ice allows the solar radiation at the end of local winter to heat up the underlying regolith during the day. This heat causes basal sublimation of the overlying ice layer, building up the air pressure underneath the ice. This pressure can be large enough to lift the ice layer and eventually break it, forming jets of pressurized CO₂ gas (Hoffman, 2002; Kieffer, 2007). The gas flux created can potentially destabilize large amounts of slope material, also underneath the ice (Pilorget & Forget, 2016). However, the requirement of slab ice means that the latter mechanism is only applicable to Martian gullies at latitudes >40°S where evidence for slab ice is observed (Dundas et al., 2017, 2019), whereas half of the observed active gully sites on the southern hemisphere are present at latitudes <40°S (Dundas et al., 2022). Furthermore, this hypothesis does not explain how the pressurized flows underneath a layer of CO₂ ice would result in the deposition of new lobate deposits and the movement of meter-scale boulders.

The second hypothesis explains the observations of fluidized granular flows via two effects within a mix of sediment and CO₂ ice tumbling down a gully (Dundas et al., 2017). The initial mass movement can be triggered by many different processes, unrelated and related to CO₂ ice sublimation, for example, dry raveling, rock fall, marsquakes, meteor impacts or CO₂ sublimation-induced slumping (Sylvest et al., 2016, 2019). In the event that a mixture of CO₂ ice and granular material starts to move, the potential energy of the fall is converted to kinetic energy that must be dissipated as heat or latent heat loss in the form of sublimating CO₂ (de Haas et al., 2019; Dundas et al., 2017; Roelofs, Conway, de Haas, et al., 2024). Furthermore, eroded and entrained sediment from the shallow subsurface or unfrosted areas could add additional heat to the mixture, enhancing sublimation (Dundas et al., 2017; Hoffman, 2002). The sublimation of the ice in the sediment-ice mixture is hypothesized to create a gas flux large enough to decrease intergranular friction and fluidize the mixture in such a way that it explains recent flows (de Haas et al., 2019; Roelofs, Conway, de Haas, et al., 2024).

Details aside, all current theories on the CO₂-driven fluidization of granular material on Mars agree on two crucial points; (a) heat is needed to sublimate the CO₂, and (b) increased pore pressure, from the CO₂ gas, in the granular material is crucial to decrease intergranular friction and cause fluidization. However, major research questions remain unanswered. First, it remains speculative whether and exactly how the sublimation of CO₂ ice is able to fluidize granular material. Second, it is unknown how much CO₂ ice needs to sublimate to explain the observed changes. Third, it is unclear how CO₂-driven granular flows on Mars create landforms that are practically identical to landforms created by water-driven debris flows on Earth. Active depositional aprons on both Earth and Mars show lobate deposits with clear levees, and contain meter-scale boulders that are transported through the gully system (de Haas et al., 2019; Dundas et al., 2022; Raack et al., 2020). The similarity in key elements in these landforms suggests similarity in the flow dynamics, but this remains unproven.

In this work, we experimentally study the fluidization of granular material by CO₂ ice sublimation under Martian conditions. We aim to (a) resolve the boundary conditions needed to fluidize granular material by CO₂ ice sublimation on Mars, (b) understand the fluid dynamics of CO₂-driven granular flows, and (c) understand and explain the similarities between the CO₂-driven granular flows and their deposits on Mars and debris-flow processes and deposits on Earth from a flow dynamics perspective.

To overcome the lack of in situ observations of CO₂-driven granular flows, we designed two experimental granular flow set-ups that were used to conduct experiments under Martian atmospheric pressure in environmental pressure chambers. In these experiments, granular flows driven by the sublimation of CO₂ in a mixture of sediment and CO₂ ice were created under different boundary conditions, that is, CO₂ content and slope, and on two different scales to understand potential scale effects. The results of these experiments provide new insights into the flow dynamics of CO₂-driven granular flows on Mars and the resulting deposit morphologies. It is

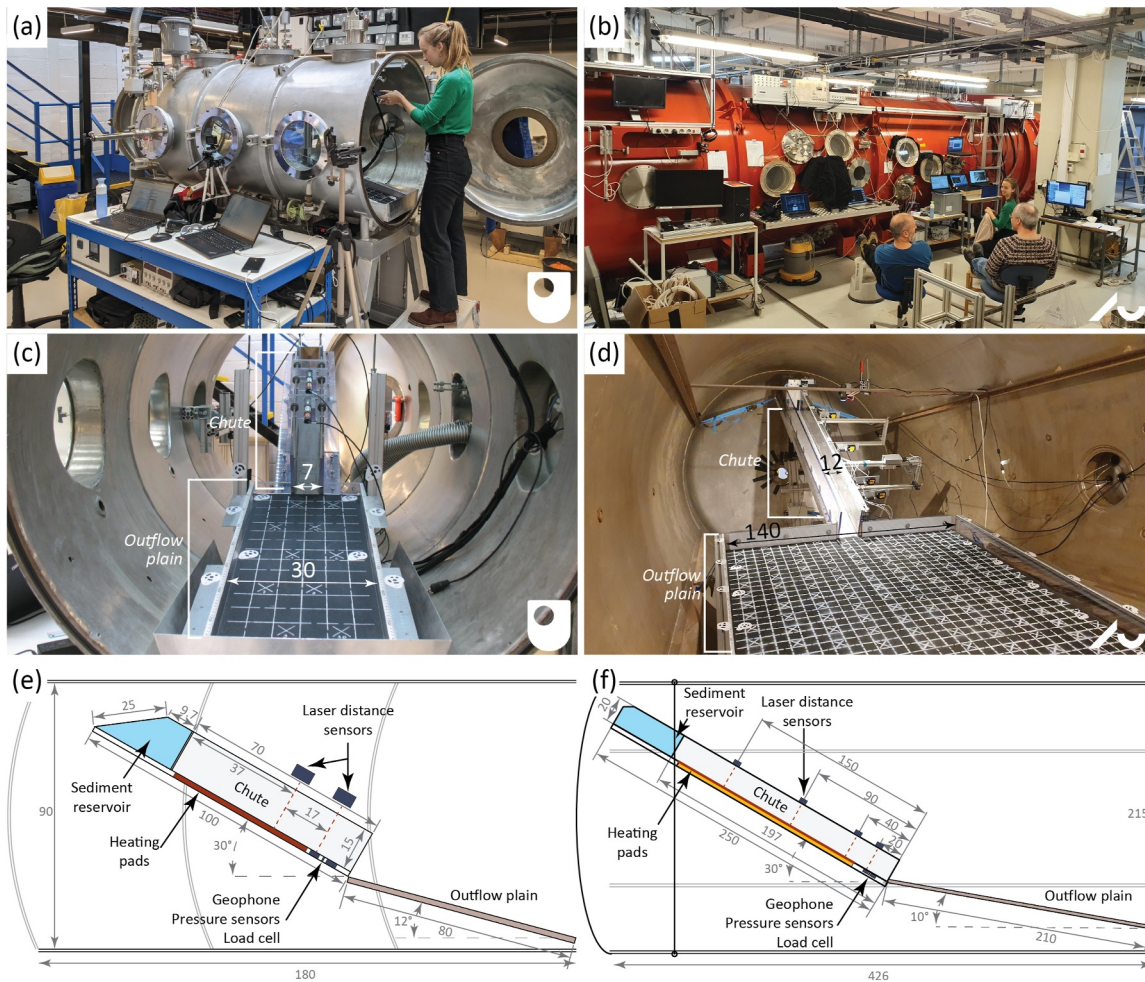


Figure 2. Photos and schematic drawings of chambers (a, b) and flumes (c–f). The photo in panel (a) depicts the Mars chamber at the Hyper Velocity and Impact lab (HVI) of the Open University (UK), panel (b) shows the Mars Simulation Wind tunnel at Aarhus University (Denmark). Details of the small-scale flume set-up used in the Mars chamber of the HVI lab can be found in (c) and (e). Details of the large-scale set-up used in the Mars Simulation Wind tunnel in Aarhus can be found in (d) and (f). All dimensions are given in cm.

important to note that with our research we specifically aim at studying the transport and deposition processes of CO_2 -driven granular flows, rather than the initiation mechanisms behind these flows.

2. Materials and Methods

To study if and how a mixture of CO_2 -ice and granular material is fluidized under Martian atmospheric conditions we designed two experimental set-ups at two different scales based on terrestrial debris flow flumes (de Haas, Braat, et al., 2015; Iverson et al., 2010; Roelofs et al., 2022). The flumes were placed in two environmental chambers of different sizes to enable us to conduct experiments under Martian atmospheric conditions (Figures 2a and 2b). Similar to terrestrial debris flow flumes, our flumes consisted of a steep and narrow chute ending on a larger outflow plain with a lower slope angle (Figures 2c–2f). The steep and narrow chute is used to study flow characteristics, for example, flow depth, velocity, and pore pressures, whereas the larger plain is used to study deposit morphology. The slope angle of the chute was varied during our experiments, whereas the slope angle of the outflow plain was kept constant (Figures 2e and 2f). As is common practice in debris flow experiments, we stored the material that makes up the granular flow in a reservoir at the top of the flume before controlled release. Using flumes of two different sizes enabled us to study possible scaling issues known to influence the behavior of experimental terrestrial debris flows (Iverson, 2015). The small-scale flume has a total length of 1.80 m and has a material reservoir that can store between 1.0 and 1.6 kg of material (Figure 2e). The large-scale flume has a total

length of 4.60 m and has a material reservoir that can store between 8.0 and 11.2 kg of material (Figure 2f). This means that, while the large flume is only a factor 2.5 longer than the small flume, the granular flow it supports is 10 times larger.

The small-scale flume was used for conducting experiments in the Mars chamber of the Hyper Velocity and Impact lab (HVI-lab) at the Open University in Milton Keynes in the United Kingdom in the autumn of 2021. The large-scale flume was used for conducting experiments in the Mars Simulation Wind Tunnel at Aarhus University in Denmark in the autumn of 2022. To compare results between the flumes, experiments were performed with similar initial and boundary conditions. In this manuscript, 46 experiments conducted in the small-scale set-up in the Mars chamber of the Open University are presented, and 15 experiments conducted in the large-scale set-up in the Mars Simulation Wind Tunnel are presented.

2.1. Chamber and Flume Details

The Mars chamber of the HVI-lab at the Open University is a cylindrical low-pressure chamber with a length of 2 m and an inner diameter of 0.9 m (Conway et al., 2011; Sylvest et al., 2016) (Figure 2a). The chamber can replicate Martian atmospheric conditions and a range of different temperatures.

The Mars Simulation Wind Tunnel at Aarhus University is a cylindrical low-pressure wind tunnel, originally designed to simulate eolian transport processes on Mars (Holstein-Rathlou et al., 2014) (Figure 2b). The chamber has a total length of 8 m and an inner diameter of 2.15 m. In both chambers, electrical and mechanical feed-throughs exist to enable the operation of the experimental set-up in the chamber from the outside. Both chambers have multiple porthole windows that allow for videography of the experiments.

Both the large-scale and the small-scale flume were mostly constructed out of Lexan, a transparent polycarbonate resin thermoplastic that can deform considerably without cracking or breaking. The transparency of the Lexan was an important design prerequisite because it allowed us to study the granular flow from the side of the chute. The bottom of the chute was created out of aluminum, with heating pads installed underneath it that controlled the temperature of the chute bottom, which was kept at 20°C during the experiments. On the edges of the outflow plain, markers were attached that were used for creating 3D models of the outflow morphologies using photogrammetry with Agisoft Metashape software. The outflow plains of the flumes were further covered with antislip material (3M Safety-Walk 500 series, equal to 80 grit sandpaper with 0.2 mm median sand diameter) to mimic natural roughness. To achieve the same for the chute bottom, the aluminum was sandblasted. The sediment and ice reservoirs on top of the flumes were constructed out of copper for the small set-up, and out of aluminum for the large set-up, because of their relatively low deformation under low temperatures. The reservoirs in both flumes are opened by means of mechanically operated trap doors. In the small-scale flume the entire reservoir opened at once, whereas in the large-scale flume, the opening height was set at 5 cm. This difference in design allowed a more constant and stable flow of granular material in the large-scale experiments, providing better insight into the flow dynamics.

In both flumes, the same sensors were used to study the flow dynamics. In the downstream part of the chute, four sensors were installed underneath the chute bottom plate (Figures 2e and 2f); a geophone (Geospace GS-20DX), two relative gas pressure sensors (Honeywell TruStability HSCDRRD006MGAA5), and a load cell (HBM PW6D —3 kg). The geophone and the load cell were attached to individual load plates of 5 by 5 cm. The geophone recorded seismic vibrations during the experiment, the pressure sensors recorded the gas pressure at the bottom of a flow relative to the ambient pressure, and the load cell recorded the weight of the granular material as the flow passed. Above the flume, multiple laser distance sensors (Baumer OADM 20U2480/S14C) were installed that recorded the flow depth at sub-mm accuracy. In the small-scale set-up two laser distance sensors were used, whereas in the large-scale set-up, four laser distance sensors were used. With the time difference of the arrival of the flow front at the different laser distance sensors, reconstructed from the flow depth data, flow velocity was calculated. In both set-ups, the last laser distance sensor was installed above the load cell (Figures 2e and 2f). This allowed us to reconstruct the density of the flow, ρ_m , according to:

$$\rho_m = \frac{M}{AH} \quad (1)$$

where M is the mass recorded by the load cell (kg), A is the area of the load cell (m^2), and H is the flow depth (m). Furthermore, by combining the load cell data and the data from the pore pressure sensors, the percentage of the material in the flows carried by the gas pressure could be quantified. The latter is a measure of the degree of fluidization. For more detailed photos of the chambers, the flumes and the sensors see Figure S1 in Supporting Information S1.

The amount of CO_2 ice sublimating during the flow in the large-scale set-up could be calculated from the data produced by a capacitance pressure sensor in the Mars Simulation Wind Tunnel. By adding the pressure draw-down caused by the pumping to the observed pressure increase during the experiment we reconstructed the amount of CO_2 released into the chamber during the flow for three individual experiments with varying amounts of CO_2 ice in the granular mixture (Figure 7).

Multiple video cameras were installed in and around both chambers. For the small-scale set-up, every experiment was recorded with a Go-Pro camera from the side and a camcorder from the front. For the large-scale set-up, every experiment was recorded with two webcams in the chamber that looked at the chute from the side, and one high-speed camera that filmed the flow at the transition from the chute to the outflow plain at a frame rate of 600 Hz.

2.2. Materials Used and Experimental Routine

Two materials form the ingredients of the granular mixture in our experiments; sand and CO_2 ice. The sand for the experiments is a mixture of fine-grained sand (silver sand of marine origin, D_{50} of 270 μm) and coarse-grained sand (builders sand of fluvial origin, D_{50} of 490 μm), combined in a specific ratio (0.6–0.4) to create a broad grain size distribution (D_{50} of 310 μm , Figure S2 in Supporting Information S1) that minimizes gas permeability relative to a mono-disperse sand, and thus slows down the gas escape rate. Furthermore, because of scaling issues related to wall effects in flume experiments, the grain size of our sediment had to be at least 20 times smaller than the chute width. Experiments conducted with only silver sand or only builders sand behave similarly overall, although finer mixtures flow further onto the outflow plain. Results of these experiments are presented in Supporting Information S1 (see Figure S7). The sand was pre-dried in the oven and cleared of any excess moisture in the environmental chambers by putting it in a vacuum prior to the experiments.

The CO_2 ice used for our experiments was ordered in pellet form from commercial parties close to the labs. To limit the contamination of the CO_2 ice with water, the CO_2 ice was stored in closed polystyrene foam containers in a sealed freezer (Figures S3a and S3b in Supporting Information S1), and the ice was refreshed at least once a week. The CO_2 ice pellets were then crushed to the size of the coarsest sand grains. For the small-scale experiments, this was done by hand with the use of a mortar and pestle. For the large-scale experiments, the ice was crushed with the KitchenAid 5KGM grain mill. Despite the difference in methods, the resulting CO_2 ice grains are similar in size and shape (see Figures S3c and S3d in Supporting Information S1).

For every experiment, CO_2 ice would be freshly crushed and mixed with a specific amount of sand. To control the amount of CO_2 ice at the start of an experiment, the combined weight was monitored during the mixing process. The loss of CO_2 due to sublimation was compensated by adding more crushed CO_2 ice. Once the desired weight ratio of sediment and CO_2 ice was reached, the mixture was poured into the sediment-ice reservoir in the flume. After this, the chamber was closed and depressurized to an atmospheric pressure of ~ 8 mbar, a process that took between 12 and 15 min in the Mars Chamber at the Open University and between 20 and 25 min in the Mars Simulation Wind Tunnel at Aarhus University. At this pressure, the mixture was released into the flume, while the sensor data was logged and the videos recorded the passing of the granular flow.

2.3. Explored Parameter-Space

To determine the conditions under which CO_2 -driven granular flows can occur on Mars, experiments were conducted under different initial and boundary conditions. For both the experiments in the small-scale and the large-scale set-up, the CO_2 -sediment ratio was systematically varied, as well as the slope of the chute. The CO_2 -sediment ratio was varied between 0 and 0.6 in the small-scale experiments and varied between 0 and 0.4 for the large-scale experiments (Table 1), while keeping the flume chute at a stable angle of 30° . Note that the mass ratio here is the ratio between the mass of the CO_2 and the sediment before depressurization of the chamber. During depressurization the CO_2 sublimates, which causes the mass ratio to change. We quantified this change for both the small- and large-scale setup by doing initial tests tracking the weight of the mixture inside the sediment-ice

Table 1
Parameters Explored in the Experiments and the Tested Values

Variable	Unit	Standard value	Tested values
CO ₂ -sediment ratio	(kg/kg)	0.3	0, 0.1, 0.2 , 0.3 , 0.4, 0.5, 0.6
Chute angle	°	30	20 , 25 , 30
Sediment type		Sand mixture	Sand mixture , Fine, Coarse
Atmospheric pressure	mbar	8	8 , 1,000

Note. All parameters and values reported in this table are tested in the small-scale setup. The values of the parameters in bold font and teal color are the ones also tested in the large-scale setup. For more details on the grain-size distributions see Figure S2 in Supporting Information S1. For a full list of all experiments see Table S1 in Supporting Information S1.

reservoir while depressurizing the chamber. The results of these tests can be found in Figure S5 of the Supporting Information S1. In the subsequent sections of this manuscript, we switch from using the initial CO₂-sediment mass ratios to using the mass fraction of CO₂ at the start of an experiment derived from these tests.

The angle of the chute was varied between 20 and 30° in both the small-scale and the large-scale experiments (Table 1), while keeping the initial CO₂-sediment mass ratio at 0.3. In the small-scale experiments, we did additional tests with different sediment types and under Earth atmospheric pressure (Table 1). To account for the effects of natural variability, each experimental setting was repeated at least twice, and when time allowed three times. A complete list of all experiments and their initial and boundary conditions can be found in Table S1 of the Supporting Information S1.

2.4. Flow Characterization

To characterize the dynamics of the CO₂-driven granular flows and objectively compare the flows of different sizes three dimensionless numbers are used; the Bagnold, Savage, and friction numbers. These numbers are used in both debris flow (Iverson, 1997; Iverson & Denlinger, 2001; Roelofs et al., 2022, 2023) and pyroclastic literature (Smith et al., 2020) and therefore also allow for comparison between the CO₂-driven granular flows, and terrestrial debris flows and pyroclastic flows. The numbers describe the relationship between the motion-resisting forces in granular flows; collisional forces, frictional forces, and viscous forces (Iverson, 1997; Iverson et al., 2010; Parsons et al., 2001). The relative importance of these forces plays a big role in both erosional (de Haas & Woerkom, 2016; Roelofs et al., 2022) and depositional processes (de Haas, Braat, et al., 2015; Zhou et al., 2019) and is, therefore, an important tool in understanding how certain flows lead to certain morphological features. The Bagnold number describes the ratio between collisional and viscous forces (Iverson, 1997):

$$Nb = \frac{v_s \rho_s \delta^2 \gamma}{v_f \mu} \quad (2)$$

wherein v_s is the volumetric solids fraction, ρ_s is the density of the sediment grains, δ is the D₅₀ (median) grain size of the sediment (m), v_f is the volumetric fluid fraction, μ is the dynamic viscosity of CO₂ gas under Martian atmospheric conditions, which is 9.82×10^{-6} Ns/m² (Bardera et al., 2020), and γ is the flow shear rate (1/s):

$$\gamma = \frac{u}{H} \quad (3)$$

wherein u is the flow velocity (m/s). According to Iverson (1997), collisional forces dominate at $N_b > 200$.

The Savage number quantifies the ratio between collisional and frictional forces:

$$N_s = \frac{\rho_s \delta^2 \gamma^2}{(\rho_s - \rho_f) g H \tan \phi} \quad (4)$$

wherein g is the gravitational acceleration (m/s^2), ρ_f is the density of the fluid, in our case this is the density of the CO_2 gas at 8 mbar, and ϕ is the internal angle of friction, assumed to be 42° (Parsons et al., 2001; de Haas, Braat, et al., 2015). The density of the CO_2 gas at a certain pressure can be calculated from the ideal gas law:

$$\rho_f = \frac{PM_m}{RT} \quad (5)$$

wherein P is the atmospheric pressure (Pa), M_m is the molar mass of CO_2 , R is the universal gas constant, and T is the temperature (K). For $N_s > 0.1$ collisional forces dominate viscous forces (Iverson, 1997). The friction number is then defined as the Bagnold number divided by the Savage number, describing the ratio between frictional and viscous forces. According to experimental data of wet experimental debris flows of Parsons et al. (2001) and de Haas, Braat, et al. (2015) frictional forces dominate over viscous forces at $N_f > 100$ for the flow body and $N_f > 250$ for the flow front.

3. Results

3.1. General Flow Behavior and Morphology

Increased fluidization of the material was observed for all experiments under Martian atmospheric pressures with CO_2 ice in the granular mixture. Compared to reference experiments without CO_2 ice, these experiments showed >2 times larger flow velocities and run-out, with typical flow velocities of 2 m/s for the small-scale flows and 3 m/s for the large-scale flows. For both the large-scale and the small-scale experiments, flow depths reached maximum values around 2 cm (Figures 3a and 3b), and flow densities around $1,000 \text{ kg/m}^3$. The relatively small flow depth in the large-scale experiments was caused by the controlled, and limited, outflow height in this setup. In both set-ups, the flow depth increased rapidly when the flow front arrived and dissipated more slowly when the tail passed. In experiments without CO_2 , as soon as the flow front arrived at the outflow plain the flow stopped and the chute backfilled with sediment.

Both the small-scale and large-scale CO_2 -driven granular flows show multiple surges (see Figures 3a and 3b and Movies S1–S11). For all flows with CO_2 in the mixture, increased gas pressures were registered at the base of the flow (Figures 3a and 3b). This gas pressure carried between 20% and 60% of the flow mass, independent of the experimental scale (Figure 3c). When analyzing the high-speed video of the experiment presented in Figure 3a it becomes clear that the velocity of the granular flow is highest in the center of the flow and that the flow itself is turbulent (see high-speed video in Movies S1–S11).

The morphology of the outflow deposits of experiments with CO_2 in the granular mixture often contain multiple lobes formed by different surges (Figure 4). These lobes are stacked on top of each other (see e.g., Figures 4c and 4l), and, in some cases, next to each other (see e.g., Figures 4f and 4k). In both the small-scale and large-scale set-up levees form in experiments where a second surge of granular material deposits on top of an earlier surge (see Figures 4b and 4f). With increased amount of CO_2 in the granular mixture the material flows further out onto the outflow plain (Figures 4a–4f). Increasing the chute slope by $5\text{--}10^\circ$ also causes the material to flow further onto the outflow plain (Figures 4g–4l). In the large-scale experiments, a small increase in slope has a larger effect on the outflow length than doubling the CO_2 content (Figures 4d–4f and 4j–4l). When no CO_2 is present in the granular mixture only a small sediment cone forms on the transition from the chute to the outflow plain.

3.2. Flow Velocity, Depth, and Pore Pressure

In the large-scale set-up, flow velocities in the lower half of the chute are constant (Figure S6 in Supporting Information S1) and reach values around 3 m/s, independent of the CO_2 fraction (Figure 5a). In the small-scale set-up, for high CO_2 fractions between 0.14 and 0.3, flow velocities around 2 m/s are recorded at the end of the chute, whereas for the lower CO_2 fractions the velocity slowly increases from 1 to 2 m/s with increasing CO_2 fraction. When no CO_2 is present in the granular mixtures, no enhanced fluidization is observed and the frontal velocity of the material is around 1 m/s in both set-ups. The same can be stated for granular flows with CO_2 in the mixture released under Earth atmospheric pressure. For both the large-scale and small-scale flows, an increase in the chute angle, from 20° to 30° , causes a small increase in flow velocity, from 2.2 to 3 m/s (Figure 5b).

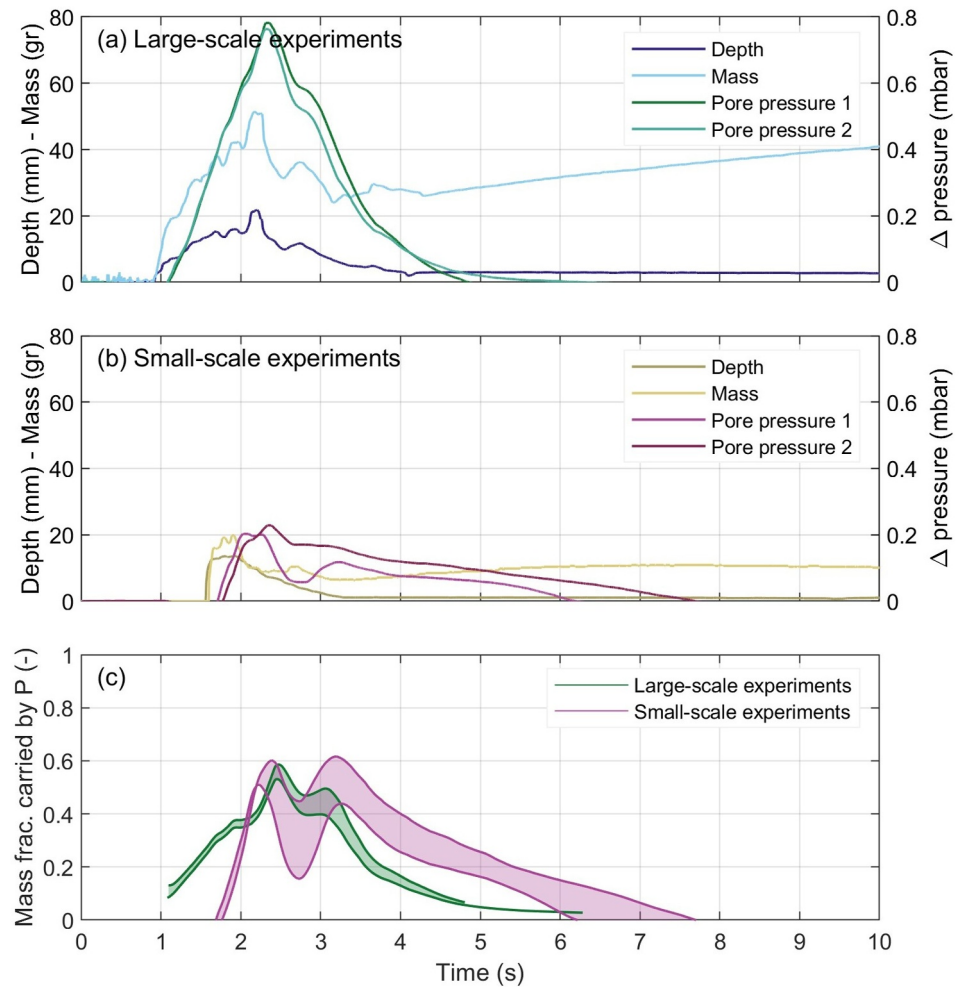


Figure 3. Example of flow depth, flow mass, and differential pore pressures (sensors 1 and 2) during an experiment for the large-scale set-up (a) and the small-scale set-up (b) with similar boundary conditions; initial CO_2 mass fraction of 0.23 and flume angle of 20° . The lower panel (c), depicts the mass fraction of the flow carried by the gas pressure for the experiments depicted in panels (a) and (b). As the data from the two pore pressure sensors slightly differs, this fraction is depicted as an envelope covering the range provided by the two sensors. The fraction carried by the gas pressure is a measure for the degree of fluidization.

Maximum flow depth increases linearly with CO_2 mass fraction for both set-ups (Figure 5c). This relation is steeper for the small-scale set-up. When increasing the chute angle, maximum flow depth decreases in the large-scale set-up from 22 to 14 mm, while staying around 15 mm in the small-scale set-up (Figure 5d). Flow depths are stable in the lower half of the large-scale flume for all experiments (Figure S6 in Supporting Information S1). In the small-scale flume, the flow depths are still increasing in the lower half of the flume, especially when the chute is on the steepest angle.

Increased basal pore pressures are observed in all experiments. Despite the large scatter in the data, caused by the sensitivity of the sensors, basal pore pressures seem to increase with increasing CO_2 mass fraction and decrease with increasing chute slope in the large-scale set-up (Figures 5e and 5f). The differential pressure signal, which is the difference between the ambient pressure and the basal pressure, is more scattered for the small-scale experiments. This is likely caused by the combination of smaller, less stable flows, and a higher amount of deposition of granular material in the chute during the experiment compared to the large-scale set-up. Maximum added pressures in the large-scale set-up vary between 0.2 and 0.6 mbar, whereas they vary between 0 and 0.4 for the small-scale set-up.

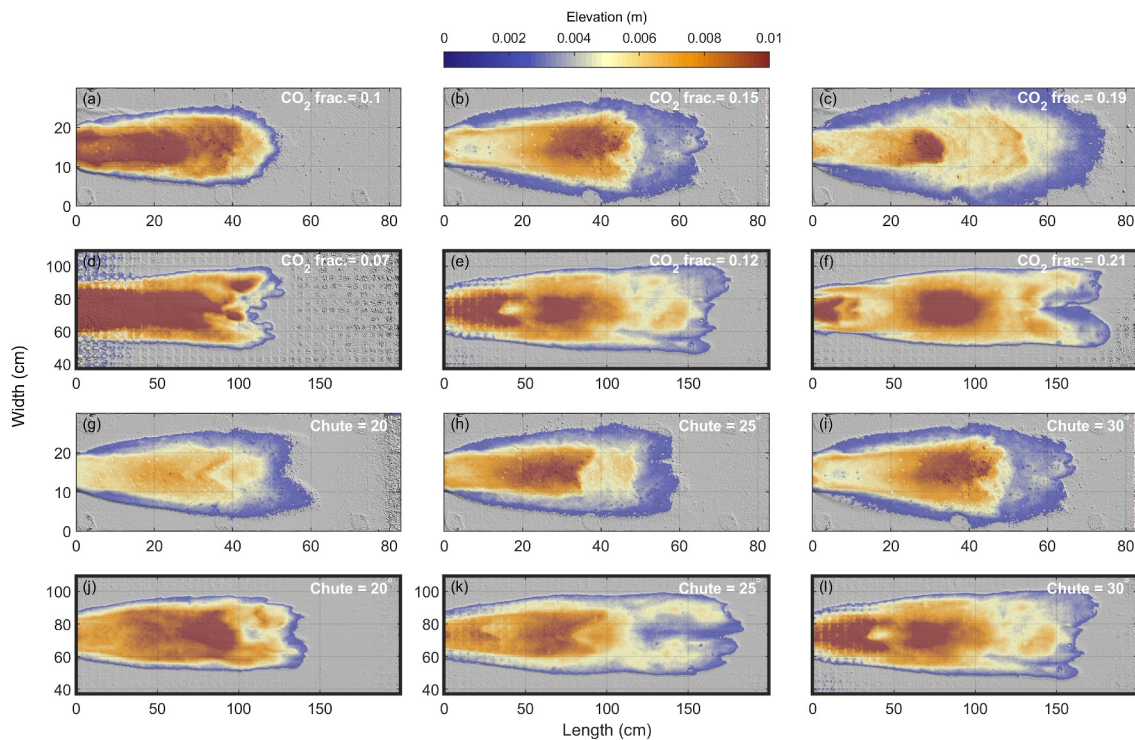


Figure 4. Digital elevation models for the outflow deposits of 12 experiments under Martian atmospheric pressures, 6 conducted in the large scale set-up, highlighted by thick black borders, and 6 conducted in the small scale set-up. The top two rows (a–f) show deposits of experiments with varying CO₂ mass fractions. The fractions depicted in the panels correspond to the mass fractions at the start of an experiment derived from Figure S5 in Supporting Information S1. The bottom two rows (g–l) show deposits of experiments with different chute angles. For all depicted experiments, videos are present in Supporting Information S1.

The type of granular material used, either silver sand, builders sand, or the mixture, did not significantly influence the flow dynamics of the flows in the small-scale set-up (Figure S7 in Supporting Information S1). Frontal velocities, maximum flow depths, and maximum basal pressure were the same for all sand types. The type of granular material used did influence the outflow deposit. CO₂-driven granular flows comprised of finer sands flowed out further (Figure S4 in Supporting Information S1).

3.3. Flow Density, Fluidization and CO₂ Sublimation During the Flow

The density of the flow is calculated from the weight data from the load cell and the depth data from the laser distance sensor above the load cell. In addition, the load cell data and the data from the pore pressure sensors are combined to calculate the percentage of the material in the flows carried by the gas pressure. Here, we only present results from the large-scale experiments, because it was not possible to calculate flow density and degree of fluidization for the experiments in the small-scale set-up due to the deposition of material on the load cell while the granular material was still flowing. Based on the combined data of the entire flow of all large-scale experiments, summarized in boxplots in Figures 6a and 6b, we can state that our experimental CO₂-driven flows have a density around 1,000 kg/m³. This density is not dependent on the CO₂ fraction (Figure 6a) but is slightly dependent on the chute angle (Figure 6b). If the angle becomes steeper, the density decreases slightly. The fraction of the flow mass supported by the gas pressure ranges between 0.2 and 0.3 on average, with a small dependency on CO₂ mass fraction (Figures 6c and 6d). For flows with a higher CO₂ fraction, a slightly higher percentage of the flow is supported by the gas pressure (Figure 6c).

The data from the capacitance pressure sensor in the chamber of the large-scale set-up shows that for an experiment with a CO₂ mass of 0.59 kg at the beginning of the experiment (Figure S5 in Supporting Information S1), only 42 g of CO₂ sublimates during the flow (Figure 7a). For a larger initial CO₂ mass of 1.12 kg (Figure S5 in Supporting Information S1), only 57 g of CO₂ sublimates during the flow (Figure 7b). During the experiments with the largest amount of CO₂ tested, with an initial mass of 2.13 kg (Figure S5 in Supporting Information S1), only 92 g of CO₂ sublimates during the flow (Figure 7c). This means that for all experiments between

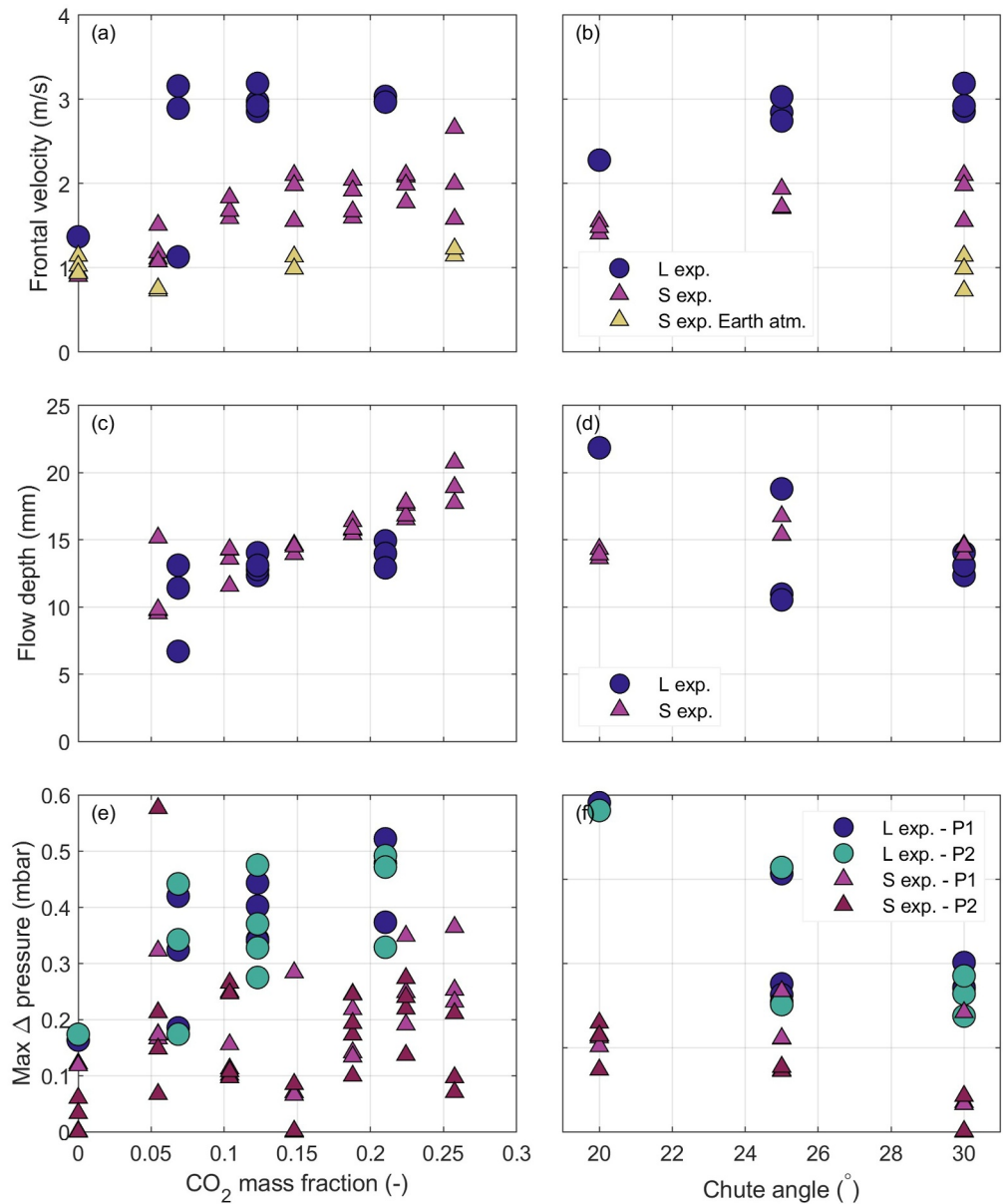


Figure 5. Frontal flow velocity (a, b), maximum flow depth (c, d), and maximum differential pore pressure for pore pressure sensor 1 (P1) and pore pressure sensor 2 (P2) (e, f), for the large-scale (L) and small-scale (S) experimental flows. All blue and purple dots represent results from experiments conducted under Martian atmospheric pressure, whereas the yellow dots represent results from experiments conducted under Earth atmospheric pressure. The results of experiments with varying CO₂ mass fractions in the flow, but a constant chute angle of 30°, are presented in the left column. Note that the mass fractions presented here are the mass fractions at the start of an experiment derived from data presented in Figure S5 of the Supporting Information S1. The results of experiments conducted under different chute angles, but with a constant initial CO₂ mass fraction of 0.33, are presented in the right column.

0.8% and 1.3% of the total flow mass (sand and CO₂ ice), and 0.5%–0.9% of the volume (assuming a porosity of 0.4) sublimates. When normalized for chute length, width, and flow duration, the volume loss is 0.3%–0.55% per m²/s, and the mass loss is 0.025–0.055 kg/m²/s.

3.4. Dimensionless Flow Characteristics

To quantitatively compare the flow dynamics of the large-scale and small-scale granular flows, we characterized the flows using the dimensionless numbers discussed in the methods; the Bagnold, Savage, and friction numbers

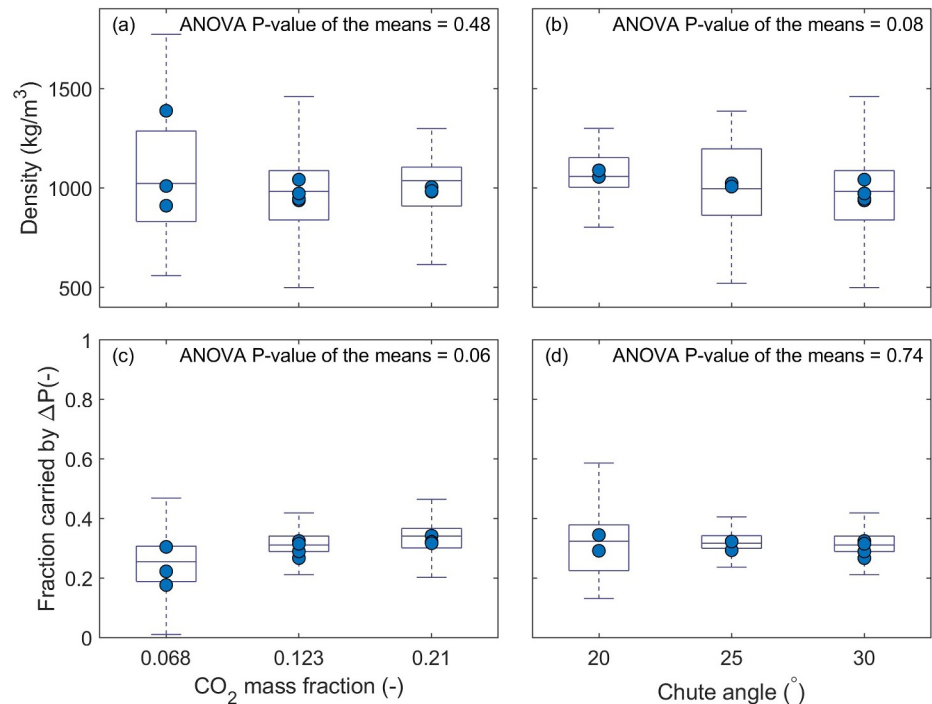


Figure 6. Boxplots showing the distribution of the flow density (a, b) and the fraction of the flow carried by the gas pressure (c, d) for the large-scale experiments conducted with different CO₂ mass fractions (left column) and under different chute angles (right column). The data in a single boxplot combines the density or fraction carried by the gas pressure of the main flow over time (flow tails are disregarded) for all large-scale experiments performed under similar conditions (i.e., similar CO₂ mass fractions and chute angle). The dark blue dots represent the mean value during one experiment. The reported p-value in the subplots stems from an ANOVA (analysis of variance) test of these means. The p-values show that the results from the different experimental groups in panels (b) and (c) are marginally significant.

(Figure 8). Furthermore, this dimensionless analysis provides the opportunity to place the flow dynamics of the CO₂-driven granular flows into the context of other granular flows, such as debris flows and pyroclastic flows. In all of our experimental CO₂-driven granular flows, frictional forces dominated over collisional and viscous forces (Figures 8c–8f). In addition, the Bagnold numbers of our flows indicate that collisional forces dominated over viscous forces (Figures 8a and 8b). The large-scale flows are relatively more collisional than the small-scale flows (Figures 8a–8d). Increasing the CO₂ mass fraction in the granular mixture does not have a large effect on the Bagnold or Savage numbers (Figures 8a–8d). However, it does affect the relation between frictional and viscous forces, making viscous forces less important (Figures 8e and 8f). An increase in the angle of the chute results in a larger relative influence of collisional forces (Figures 8b and 8d).

4. Discussion

4.1. Initial and Boundary Conditions for CO₂-Driven Flows

Our experiments show that granular material can be fluidized by sublimating CO₂ ice under Martian atmospheric conditions (Figures 3 and 5). This is enabled by the low Martian atmospheric pressure of around 8 mbar, which makes the gas flux from sublimation large enough to decrease intergranular friction between the grains and fluidize the granular material (Figure 5) (Cedillo-Flores et al., 2011; de Haas et al., 2019). Under terrestrial atmospheric pressure of around 1,000 mbar, sublimation of CO₂ ice still occurs, but the gas flux from the ice into the atmosphere is not large enough to decrease intergranular friction and fluidize the granular material. From our experiments, it can be inferred that the fluidization induced by the sublimation of CO₂ ice grains in a granular mixture can sustain a stable fluidized flow in a channel, that is, the flume chute, as long as CO₂ ice is present and enough energy is available for sublimation. In our experiments, less than 10% of CO₂ ice in the mixture sublimated while in the chute, implying that the mixture could have likely flowed in a sustained fluidized way in a confined chute with a length of ~10–20 m.

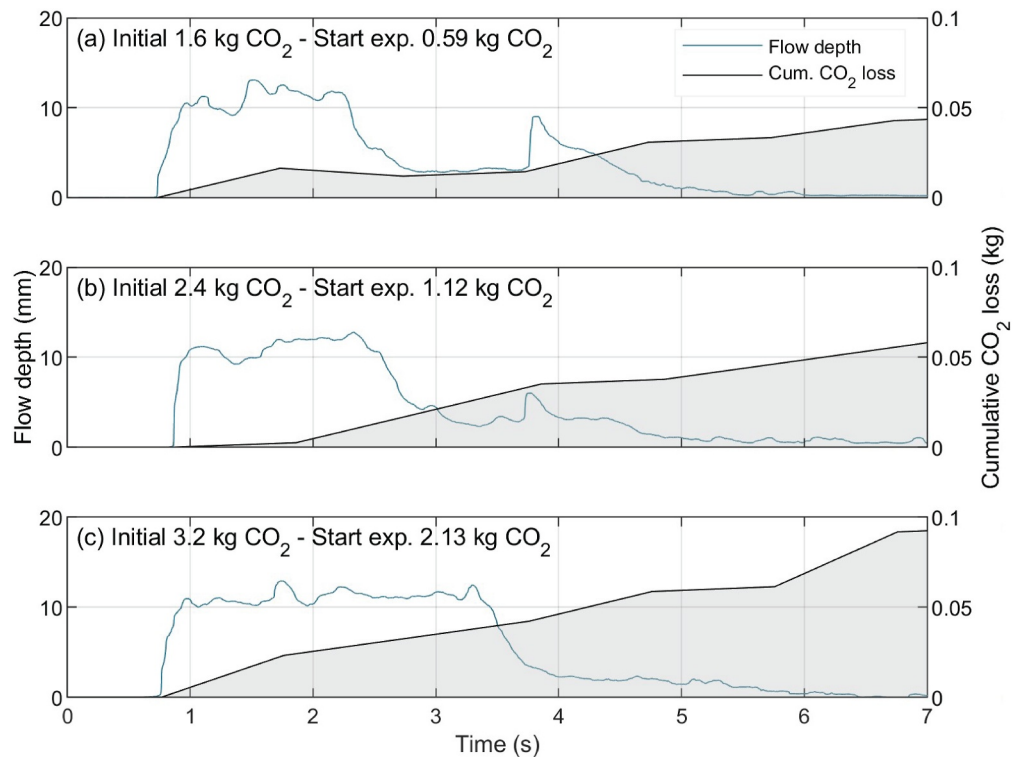


Figure 7. Flow depth and cumulative CO₂ mass loss for three experiments in the large-scale set-up, with a CO₂ mass at the beginning of the experiment of (a) 0.59 kg, (b) 1.12 kg, and (c) 2.13 kg. All experiments were conducted under a chute slope of 30°. The cumulative CO₂ mass lost is determined based on data from a capacitance pressure sensor in the chamber, the measurement frequency is 1 Hz.

The fluidization of the material by the sublimation of CO₂ ice in the chute is reflected in the enhanced frontal flow velocities and increased basal pressures (Figure 5). In experiments under Martian atmospheric conditions, where CO₂ ice is present in the granular mixture, velocities between 2 and 3 m/s are reached, whereas frontal velocities in experiments without CO₂ ice, or with CO₂ ice under Earth atmospheric pressure, are only 1 m/s (Figure 5). Furthermore, the pressure data show that the gas pressure carries between 20% and 60% of the total flow mass in the experiments with CO₂ ice (Figures 3c and 6).

In the large-scale experiments, stable flow velocities around 3 m/s are reached in the lower part of the chute for all experiments, even for the experiments with the smallest amount of CO₂ ice in the mixture. This implies that for all the different CO₂ ice fractions tested, the rate of fluidization is high and comparable, which is supported by only small differences in the amount of the flow carried by the pore pressure (Figure 6). Therefore, we hypothesize that granular material can be fluidized by the sublimation of even smaller amounts of CO₂ ice than we tested. In the small-scale experiments, we do see an increase in flow velocity and fluidization rate for the smallest CO₂ ice fractions (Figure 5a), which would imply a higher fluidization rate for larger CO₂ ice fractions. However, we hypothesize that this trend is likely caused by the limited length of the chute compared to the distance over which the flow accelerated, instead of an actual relation between CO₂ fraction and velocity in our small-scale set-up. The longer chute length in our large-scale set-up allows the flow to reach a stable state where a balance exists between CO₂ ice sublimation, the reduction in friction because of the induced gas pressure, and the remaining friction, as we see in the large-scale set-up.

Our experiments also show that CO₂-driven granular flows are fluidized enough to flow on slopes below the angle of repose. CO₂-driven flows in experiments with chute angles of 20° still reach velocities 2 times higher than those of dry granular material without CO₂. In addition, the CO₂-driven flows continue to flow over the outflow plain of our set-ups, which have even lower slope angles, 10° and 12° for respectively the large-scale and small-scale set-ups. However, as the flow on these outflow plains is unconfined, the granular material spreads out laterally and ultimately halts (Figure 4). The lateral spreading decreases the flow depth and increases the relative

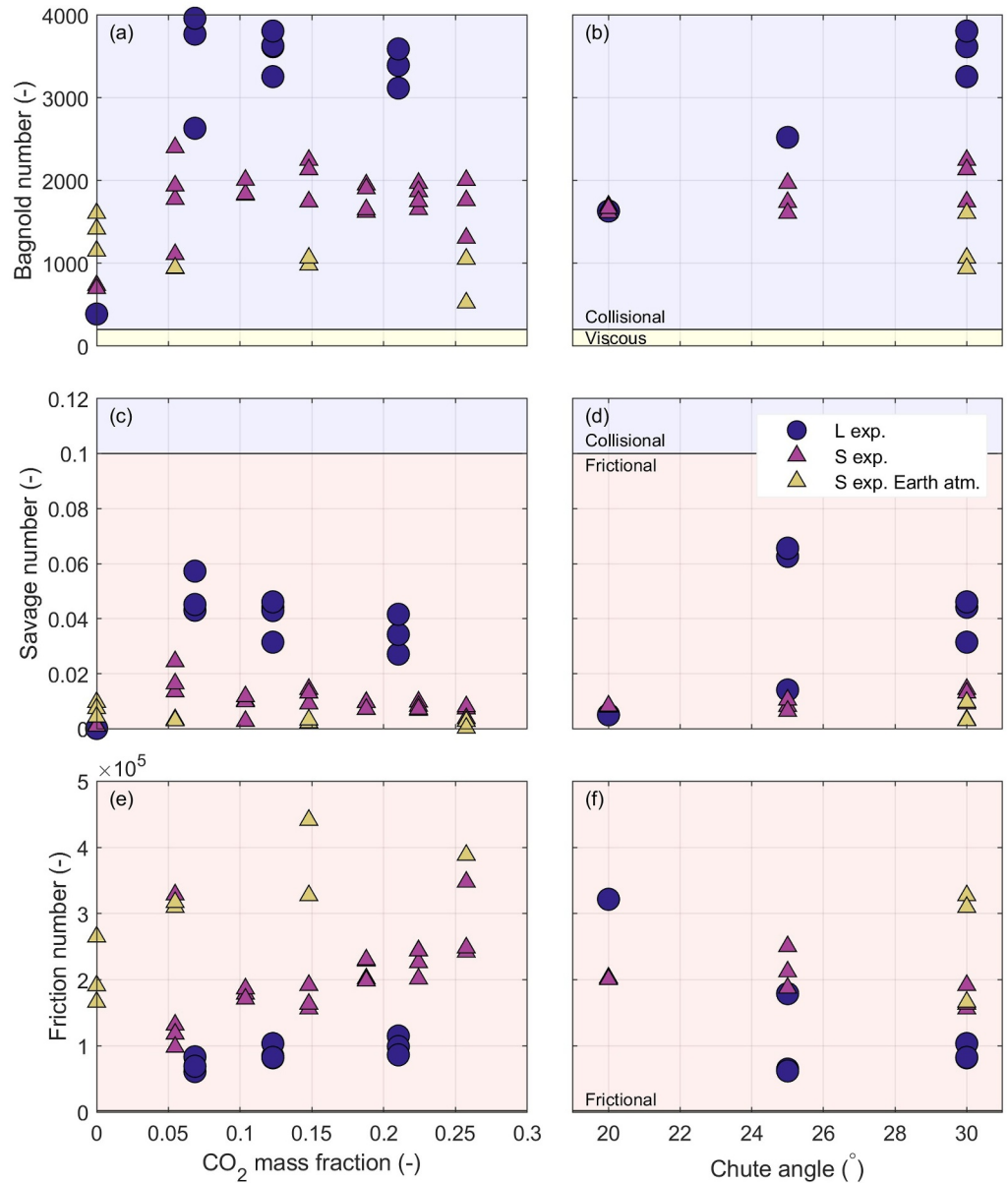


Figure 8. Bagnold (a, b), Savage (c, d), and friction (e, f) numbers for the granular flows in the large-scale and small-scale experiments conducted with different CO_2 mass fractions (left column) and under different chute angles (right column). The horizontal lines indicate the transition from one flow regime to the other (Iverson, 1997). For the Bagnold number (a, b), this is the transition between the collisional and the viscous flow regime. For the Savage number (c, d), this is the transition from the collisional to the frictional flow regime. For the friction number (e, f), this is the transition from the frictional to the viscous flow regime, the latter is not visible in the plot because the flows are far into the frictional flow regime.

amount of friction the flows have to overcome, both by increasing the area for gas escape and increasing the contact between the flow and the surface. These experimental observations on fluidization on slopes below the angle of repose are important because they support the hypothesis that CO_2 -driven flows on Mars can cause the changes we observe, like new depositional lobes on aprons with slopes as low as 10° – 15° (Diniega et al., 2010; Raack et al., 2020; Sinha & Ray, 2023).

The data from the pressure sensors in the chamber of the large-scale set-up highlight that the mass of CO_2 ice that needs to sublimate for the fluidization process is small. For example, to fluidize 8 kg of sand in our experiments, as little as 43 g of CO_2 ice needs to sublimate, equal to $\sim 0.5\%$ of the volume fraction of the flow (Figure 7). In

other words, in our experiments, a mass loss of sublimating CO₂ ice between 0.025 and 0.055 kg/m²/s is enough to create fluidized granular flows.

4.2. Heat Transfer From the Environment to the CO₂ Ice

Our experiments clearly show that granular material can be fluidized by sublimating small amounts of CO₂ ice, less than 1% of the total flow weight, under Martian atmospheric conditions when sufficient energy is available for CO₂ ice sublimation. However, where that energy is coming from on Mars is debated. According to Dundas et al. (2017) and de Haas et al. (2019), this energy could be provided by the release of kinetic energy of a fall or from heat from warmer material in contact with the granular mixture of CO₂ ice and sediment. The sublimating ice would consequently increase pore pressures in the involved granular material, which would cause fluidization and a two-phase granular flow. If all potential energy of a fall of 300 m, as earlier used by Dundas et al. (2017), would be transferred to heat according to:

$$E_p = mgL \quad (6)$$

with m as the mass of the material falling (kg), g the gravitational acceleration on Mars (3.71 m/s²), and L being the fall height, the total available potential energy, E_{pot} , would equal to 1,113 J per kg material. For our flume set-ups, the total potential kinetic energy is smaller, with 16.7 J/kg in the large-scale set-up and 5.9 J/kg for the small-scale set-up. However, the enthalpy of sublimation of CO₂ ice, which is the energy needed for the phase transition from ice to gas, is around 26–28 kJ/mol (Cedillo-Flores et al., 2011; Shakeel et al., 2018; Stephenson, 1987), which is equal to an energy of 590–636 kJ/kg, accounting for the molecular mass of CO₂ of 44.01 g/mol. This implies that in our experimental set-ups, the available potential energy could, at maximum, be responsible for the sublimation of 0.01–0.028 g of CO₂. Although a more substantial amount of sublimation due to potential energy conversion could be possible in real Martian gullies, the energy conversion will not happen instantaneously but will occur progressively as material tumbles down the slope. Therefore, we hypothesize, as Dundas et al. (2017) did earlier, that the heat from the environment, thus from warmer material and surfaces in contact with the flow, is the main driver of sublimation instead of kinetic energy conversion.

Granular material at a slightly higher temperature than the CO₂ frost point could make several thousands of J/kg available (Dundas et al., 2017). To put numbers to this, for our flumes the energy available in the aluminum bottom plate to sublimate CO₂ ice at the frost point temperature can be calculated as follows:

$$E_t = mc\Delta T \quad (7)$$

with m the mass of the aluminum, c the specific heat (902 J/kgK) and ΔT the temperature difference between the temperature of the chute bottom (20°C, or 293 K) and the CO₂ frost temperature (−120°C, or 153 K, at 8 mbar atmospheric pressure). For our small-scale flume E_t is 67 kJ, and for our large-scale flume E_t is 324 kJ. If all this thermal energy is used to sublimate CO₂ ice, between 0.51 and 0.54 kg of CO₂ ice could sublimate in our large-scale set-up and between 0.1 and 0.11 kg of CO₂ ice could sublimate in our small-scale set-up. The predicted mass of CO₂ that could sublimate as a result of heat energy in our large-scale flume is similar to the actual observed mass of CO₂ ice that sublimated during the flows (Figure 7).

Equation 7 can also be used to estimate the amount of potential thermal energy available for sublimation at the bottom of a hypothetical gully on Mars. Taking two gullies in Hale crater, as representatives for Martian crater gullies in general, studied by de Haas et al. (2019), as an example; we state that our hypothetical Martian gully is incised in basaltic bedrock ($c = 600$ J/kg°C, $\rho_{basalt} = 3,000$ kg/m³), has a length of 600 m, a width of 15 m, and in the gully, the upper 1 mm of the surface regolith is heated up to a temperature of 20°C, which is realistic for active gullies according to climate modeling (Roelofs, Conway, de Haas, et al., 2024). In this gully system, the total potential thermal energy equals 2.27×10^6 kJ. If all this energy is used to sublimate CO₂ ice, between 3,570 and 3,840 kg of CO₂ at frost temperature could be sublimated. Suppose we combine the sublimating ice-to-sediment ratio in our experiments, of 0.5%–0.9%, with this estimated CO₂-ice mass for extrapolation purposes. In that case, we can estimate that between ~396,000–~769,000 kg and ~247–~480 m³ of unconsolidated granular material could be fluidized in this Martian gully when enough ice is available. Although this estimate is likely too conservative because it does not account for the weaker Martian gravity and the possible entrainment of warmer

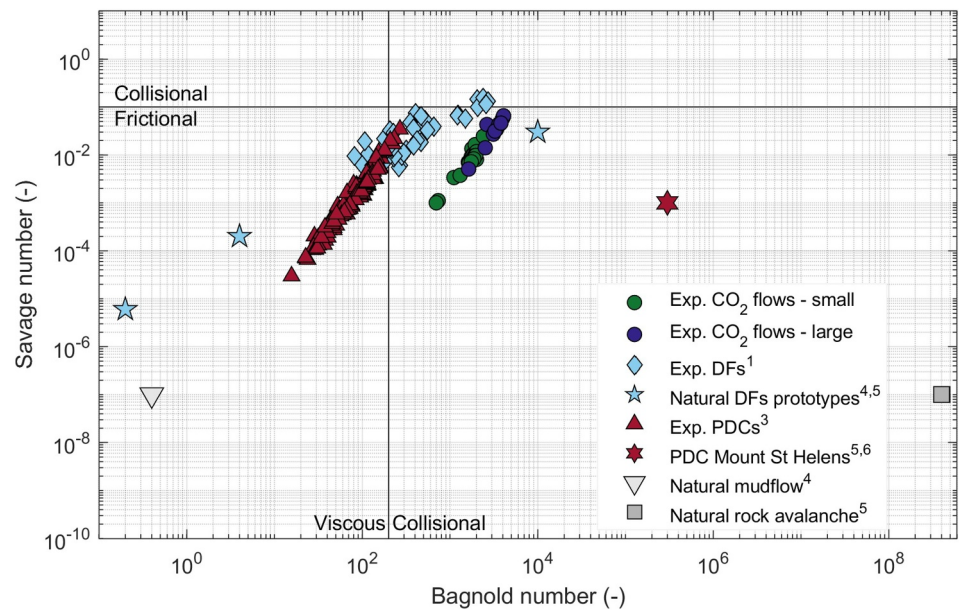


Figure 9. Bagnold numbers plotted against Savage numbers for the experimental CO₂-driven flows presented in Figure 4, the experimental debris flows from Roelofs et al. (2022)², the experimental dense pyroclastic density currents from Smith et al. (2020)³, three prototype natural debris flows from Iverson (1997)⁴ and Iverson and Denlinger (2001)⁵, a natural mud flow from Iverson (1997)⁴, a rock avalanche from Iverson and Denlinger (2001)⁵, and a pyroclastic density current from Mount St Helens from Iverson and Denlinger (2001)⁵ and Rowley et al. (1981)⁶.

sediment, the prediction matches the back-calculated flow volumes of 415 and 263 m³ in the smaller gullies in Hale crater (de Haas et al., 2019).

In general, our experimental granular flow results on thermal energy, flow volume, and the necessary mass of CO₂, agree with the back-calculated numbers for actual Martian flows (de Haas et al., 2019). Nonetheless, our predicted E_t neglects important parameters and processes in thermodynamics. In the first place, it assumes that all heat is converted to energy for sublimation during the flow. This is unlikely because heat transfer does not happen instantaneously and is dependent on the type of heat transfer, the duration of the potential transfer, and the materials involved. The heat transfer process is further complicated by the newly found turbulent behavior of CO₂ driven flows, the presence of multiple materials, the unknown areas of contact between the cold ice and the warmer materials, and the possible entrainment of warmer material into the flow (de Haas et al., 2019). Furthermore, for experiments, this E_t does not account for the constant heat input into our flume from heating pads installed underneath the aluminum bottom plate. Despite the still unresolved complications, the predicted thermal energy is multiple orders of magnitude larger than the potential energy transformed from a fall, both in our flumes as in our hypothetical gullies on Mars. The heat energy from the environment, either transferred by conduction, radiation, or convection, is, therefore, more likely to be the cause of the sublimation of the CO₂ ice in CO₂-driven granular flows on Mars. This implies that CO₂-driven granular flows can only occur in gullies on Mars at specific locations and during specific periods during the Martian year when CO₂-ice and warmer regolith simultaneously exist in the gully (Roelofs, Conway, de Haas, et al., 2024).

4.3. Flow Dynamics and Morphology of CO₂ Driven Martian Flows in (Terrestrial) Context

To enable a fair comparison between the flows in the two different experimental set-ups, and compare our CO₂-driven flows with other two-phase granular flows we conducted dimensionless analysis. This analysis shows that the CO₂-driven flows in our experiments are supercritical two-phase flows (see Froude numbers in Figure S8 of the Supporting Information S1) in which frictional forces dominate, and collisional forces are more important than viscous forces (Figure 8). In experimental and real debris flows, frictional forces typically dominate (Iverson, 1997; Iverson & Denlinger, 2001; Roelofs et al., 2022, 2023) (Figure 9). In experimental dense pyroclastic density currents, frictional forces dominate, and viscous forces seem to be more important than collisional forces (Smith et al., 2020) (Figure 9). The latter could stem from the relatively small grain size between 45

and 90 μm used by Smith et al. (2020) in their experiments. As far as we found, for only one natural pyroclastic density current the dimensionless numbers are known, and for that specific flow, the collisional forces seem to dominate over viscous forces (Iverson & Denlinger, 2001; Rowley et al., 1981) (Figure 9).

Despite the variation between the relative importance of certain forces between pyroclastic density currents, debris flows and our experimental CO_2 -driven granular flows, these different multi-phase flows show similarity in dynamics, especially considering the variability within one flow group. The similarity becomes even more evident when comparing the dynamics of debris flows, dense pyroclastic density currents, and CO_2 -driven flows with the dynamics of mud flows or natural rock avalanches (Figure 9). For both natural mud flows and rock avalanches, frictional forces are 10^2 – 10^6 higher than natural and experimental debris flows, dense pyroclastic density currents, and our CO_2 -driven granular flows. In addition, in mud flows, the viscous forces become more dominant over collisional forces than for the other flows, and in rock avalanches, collisional forces become 10^3 – 10^7 more dominant over viscous forces.

The similarity in the relative influence of different forces in the flow between our CO_2 -driven granular flows, and other fluidized multi-phase flows on Earth, is reflected in the similarity in the morphology of the deposits. The deposits of our experiments are lobate in shape, often show splitting of lobes, and sometimes have levees, similar to the hypothesized CO_2 -driven granular flow deposits on Mars (Conway et al., 2019; Hugenholtz, 2008; Johnsson et al., 2014; Lanza et al., 2010; Levy et al., 2010; Sinha et al., 2018). These morphological elements are also observed in debris flow deposits (Blair & McPherson, 1998; de Haas, Kleinhans, et al., 2015; de Haas et al., 2018; Hubert & Filipov, 1989) and pyroclastic flow deposits (Jessop et al., 2012; Lube et al., 2007; Rowley et al., 1981), whereas they are less pronounced in mudflow deposits and absent in rock avalanche deposits (Figure 10). Not all of our outflow deposits contain different distinct lobes or levees, but nor do all recent deposits in gullies on Mars. A lack of levees might indicate a lack of clear grain size segregation, which is believed to contribute to levee formation (Baker et al., 2016; Jessop et al., 2012; Johnson et al., 2012). This could be caused by a more narrow grain size distribution or a relatively smaller influence of collisional forces over viscous forces. The latter can stem from a relatively small median grain size or high shear rates (see Equation 2). Another factor that could influence the absence of levees in most of the lobes in our experimental work is the limited amount of surface friction and the inability of pore pressures to dissipate into the substrate and for particles to interact with the substrate. Earlier experimental work on terrestrial debris flows has shown that when experimental debris flows deposit on a layer of permeable sand the formation of levees is promoted (de Haas, Braat, et al., 2015).

4.4. Scaling and Upscaling to Mars

From experiments with debris flows we know that small-scale flows experience larger effects of yield strength, viscous flow resistance, and grain inertia than field size flows (Iverson, 1997, 2015; Iverson & Denlinger, 2001; Iverson et al., 2010). In addition, for small-scale experimental debris flows it has been proposed that they are insufficiently affected by pore-fluid pressure (Iverson, 1997; Iverson & Denlinger, 2001; Iverson et al., 2010). However, certain steps can be, and were, taken to overcome these scaling problems and use small-scale experiments for valid representation of real-world phenomena. For example, when scaling for momentum, a steeper slope in granular flow experiments can induce larger flow velocities to combat the effects of a smaller flow mass. Furthermore, it is important to evaluate the validity of experimental findings for the natural world by comparing flow dynamics expressed in dimensionless analysis. From the dimensionless analysis performed and discussed in the section above we can state that our CO_2 -driven granular flows behave dynamically similar to debris flows and pyroclastic forms on Earth, both on an experimental and field scale (Figure 9). In addition, our experimental CO_2 -driven granular flows show similar flow behavior to those of back-calculated CO_2 driven flows in Hale crater (de Haas et al., 2019), with similar fractions of CO_2 needed for fluidization, and similar flow velocities around 3 m/s in the steepest parts of the gullies and run-outs on slopes ranging between 13 and 19°.

The different sizes of the two experimental set-ups allow an assessment of the influence of scaling on CO_2 -driven flows. From the dimensionless scaling in Figure 8, we can see that in our large-scale set-up, the collisional forces in the flow are of a higher importance than in the flows in the small-scale set-up. This difference is linked directly to the design of the opening mechanism in the large-scale flume, which limits the flow depth relative to the flow velocity more than in the small-scale flume. Due to the restriction of the flow height, and therefore a restriction of the outflow discharge, the flow depth stays artificially low in the chute. This is reflected in a higher share rate γ , see Equation 2, and thus a larger importance of collisional forces. Additionally, we see that the friction number of

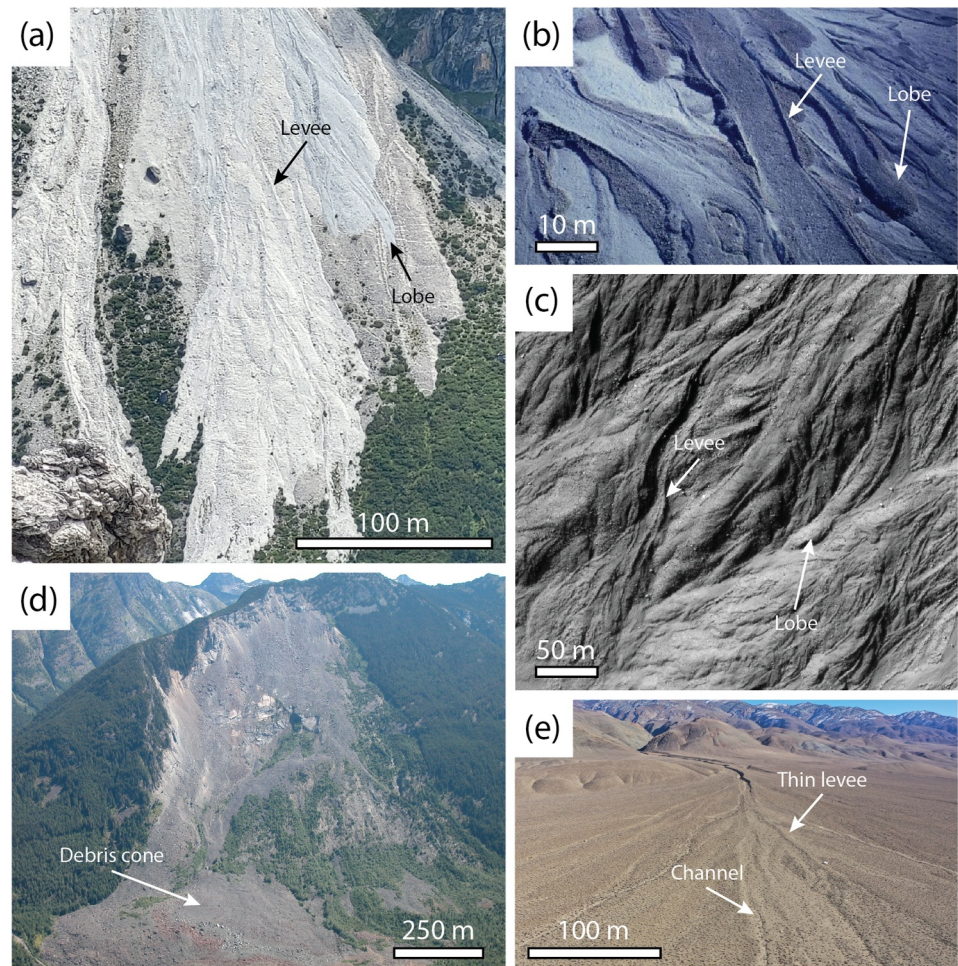


Figure 10. Different natural granular flows and their key morphological features. (a) Debris flow fan with different lobate deposits with levees near Pinnisalm, Neustift im Stubaital, Austria. (b) Pyroclastic density current deposits from the eruption of Mount St Helens in 1980 on July 22, showing multiple channels with levees and lobes (Photo: Dan Miller and USGS, first published in Baker et al. (2016)). (c) Granular flow deposits on the slopes of Istock crater on Mars with levees and lobes (Photo: NASA—HiRISE PSP_006837_1345) (Johnsson et al., 2014; de Haas, Hauber, et al., 2015) (d) Rock avalanche Hope Slide, Hope, British Columbia, Canada (Photo: John Clague). (e) Mud flow dominated Coldwater Canyon fan, California, USA, showing channels and dispersed lobes with thin levees.

our flows in the large-scale set-up is smaller than those in the small-scale set-up. Although significant differences in the dimensionless numbers between the large- and small-scale flows exist, they are small compared to differences in dimensionless numbers of experimental debris flows in the same flume but of different compositions (Roelofs et al., 2022, 2023) or of experimental pyroclastic density currents in the same flume but for different aeration states (Smith et al., 2020).

To summarize, the flow dynamics and morphology of our experimental CO₂-driven flows are comparable to a variety of natural two-phase flows (Figures 4, 9, and 10) and the influence of scale-effects on our experimental CO₂-driven flows seems to be relatively small. Classical scaling problems in debris flow experiments, related to viscous flow resistance, interstitial fluid, and pore pressures, are of a smaller concern in our CO₂-driven flow experiments because of the scale independence of the CO₂ sublimation process, pore pressure, and flow depth (de Haas et al., 2019; Roelofs, Conway, de Haas, et al., 2024), and the low viscosity of the CO₂ gas. Therefore, our findings are of direct relevance to full-scale CO₂-driven flows on Mars.

On Mars the gravitational acceleration is 3.71 m/s², and thus 2.6 times smaller than on Earth. This could possibly influence the flow dynamics of CO₂ driven granular flows. We partly accounted for the smaller gravity on Mars by conducting our experiments on multiple slopes, and therefore studying how the changing gravitational

component driving our flows would affect the results. However, the most important driver of CO₂-driven flows is the sublimation of the CO₂ frost, which is independent of gravity. The effect of gravity comes into the equation in the form of the weight of the particles in the flow and the speed with which they fall back to the surface. As earlier described by Roelofs, Conway, de Haas, et al. (2024), the extent to which the flow is suspended is given by a dimensionless group, which describes the ratio of the Darcy pressure $Hq\mu/\delta^2$ to the weight of the flow $Hg\rho_m$;

$$\frac{Hq\mu}{Hg\rho_m d^2} = \frac{q\mu}{g\rho_m \delta^2}. \quad (8)$$

where q is the volume flux of CO₂ in m/s. Here ρ_m and μ are the same for our experiments and Mars while g is different on Mars, but this can be compensated by increasing the grain diameter δ or decreasing the sublimation flux q by the same factor.

The equation above implies that under Martian gravity only 0.38 of the volume flux of CO₂ is needed compared to Earth to fluidize a flow or that with the same amount of sublimating CO₂ ice significantly larger grains can be transported on Mars. Practically this means that under Martian gravity, if we were to repeat our large-scale experiments, we would be able to decrease the amount of CO₂ used to fluidize 8 kg of sediment over the length of our flume from 42 to 16 g, equal to a volume fraction of ~ 0.002 . This falls in the volume fraction range, 2×10^{-2} – 2×10^{-5} , predicted to be needed for recent gully flows in Hale crater (de Haas et al., 2019). Furthermore, the sustained fluidization under varying chute and outflow plain angles gives us the experimental evidence that under a range of gravitational accelerations sublimating CO₂ ice can produce two-phase granular flows.

4.5. Implications for Martian Landscape Evolution and Granular Flows in the Solar System

From extensive analysis of remote sensing data we know that Martian gullies are active landscape features. Dundas et al. (2019), Pasquon et al. (2019), Dundas et al. (2022), and Sinha and Ray (2023) observed erosion and transport of material in gullies, the formation of new terraces and erosion of channel segments, the migration of sinuous curves, channel abandonment, and lobate deposits. Dundas et al. (2019) also observed early stages of gully initiation, suggesting that the processes shaping and changing the gullies today are not merely modifying the pre-existing landforms, but are capable of actively shaping the landscape. Despite these observations, it remains debated what the original formation process of these landforms is. Our experimental results support the hypothesis by Diniega et al. (2010) and Dundas et al. (2012, 2015, 2019, 2022) that current activity, by granular flow processes driven by CO₂ sublimation, are actively forming Martian gullies, and are not merely modifying older water-formed features, as suggested by Dickson et al. (2023).

The similarity in flow dynamics and morphology between our experimental CO₂-driven granular flows and natural two-phase granular flows on Earth supports their landscape-changing potential. On Earth, the erodible power of debris flows is suggested to be a primary force in cutting valleys in steep landscapes (Stock & Dietrich, 2003). Although the erodible power of CO₂-driven granular flows has yet to be experimentally explored, the observations of the Martian surface (Dundas et al., 2019, 2022; Sinha & Ray, 2023) and the observed dynamics of the experimental flows leave little doubt that erosion of material by CO₂-driven granular flows is possible. With the current state of remote observations and the lack of detailed in situ sedimentological and geological investigations, it is impossible to completely rule out a water-driven origin of the Martian gullies. However, we need to be cautious about assuming a water-driven past for the Martian gullies when CO₂-related processes can explain present-day gully activity. As most gullies on Mars were formed during the Amazonian period on Mars, when little to no liquid water could exist on its surface, we deem it likely that the gullies on Mars have been modified and possibly formed by CO₂-related processes for the past 1–3 Ga.

For other planetary bodies in our solar system, our experimental results emphasize that the existence of gully like landforms is not definite proof of flowing liquids. For example, the observed gully landforms on Vesta (Scully et al., 2015) and Mercury (Rothery et al., 2020) could also have a sublimation-related formation process, especially because of the lack of atmosphere of both bodies. Therefore, our results raise an important question on the use of Earth analogs for planetary science. Earth analogs have been essential in the exploration and understanding of planetary surfaces in our solar systems as well as the potential habitability of these planetary surfaces. Analog studies are the backbone of our understanding of the processes that shaped the surfaces of rocky planets and

bodies throughout our solar system. However, the pitfall of Earth analog studies is the combined problems of unknown-unknowns and equifinality. The latter principle describes that different processes can result in the same outcome. Our experimental results contribute quantitatively toward a fundamental reinterpretation of planetary landforms previously thought to be formed by flowing liquids.

5. Conclusion

We experimentally investigated the feasibility of CO₂-ice sublimation as the driving force in fluidized granular flows on Mars. We conducted 68 experiments under Martian atmospheric conditions in two set-ups on different scales to explore under which boundary and initial conditions granular material can be fluidized by the sublimation of CO₂-ice.

Our experiments show that under Martian atmospheric pressure of 8 mbar, the sublimation of small quantities of CO₂-ice, ~0.5% of the total flow volume, can fluidize large volumes of granular material on a range of different slopes, as long as enough thermal energy is present to initiate the sublimation of the CO₂-ice. Under Martian atmospheric pressure, the sublimation of CO₂-ice in a granular mixture increases the pore pressure within the flow by 0.2–0.6 mbar. This increased pressure carries a significant portion of the total weight of the flow, between 20% and 60%, which indicates a decrease in granular friction between the grains and a high degree of fluidization of the mixture. The fluidization of the material results in large flow velocities that exceed velocities in dry granular flows by a factor 2–3.

Dimensionless analysis of the CO₂-driven flows shows that they are dynamically similar to debris flows and dense pyroclastic density currents on Earth. The flows are supercritical and turbulent in behavior, and frictional forces dominate over collisional and viscous forces. The similarity in flow dynamics is reflected in the similarity in deposit morphology. The gully deposits on Mars, and the deposits of our experimental CO₂ driven flows contain morphological elements, like levees and lobes, that are seen as key characteristics of debris flow and pyroclastic flow deposits. In addition, our findings on flow dynamics and morphology of CO₂ driven flows support the earlier proposed hypothesis that CO₂-driven processes are actively modifying and forming Martian gullies today.

The dynamic similarity between CO₂-driven granular flows on Mars and water-driven debris flows on Earth makes it very likely that the CO₂-driven process can explain the evolution of these landforms on Mars during the Amazonian, when little to no liquid water was present on the surface of Mars. As debris flows driven by water form gully landforms on Earth, it is reasonable to assume that CO₂-driven granular flows, with similar flow dynamic properties, can form gully landforms on Mars.

Furthermore, our calculations highlight the importance of thermal energy in driving the sublimation of CO₂-ice that propels the fluidization of granular material. Direct thermal energy is a far more effective source of energy for sublimation than the conversion of kinetic and potential energy from a fall to heat. This implies that it is likely that CO₂-driven granular flows can only occur in gullies on Mars at specific locations and during specific periods during the Martian year when CO₂-ice and warmer regolith simultaneously exist in the gully.

Lastly, our experimental results emphasize that the existence of gully like landforms on planetary bodies is not definite proof of flowing liquids. Gully landforms could also be formed by or at least be altered by sublimation-related processes.

Data Availability Statement

For all the experiments presented in this manuscript, the data collected by the sensors in the flumes and the DEMs of Difference, along with a list of the experimental conditions and instructions on how we processed the raw data can be found in Roelofs, Conway, van Dam, et al. (2024).

References

- Baker, J., Gray, N., & Kokelaar, P. (2016). Particle size-segregation and spontaneous levee formation in geophysical granular flows. *International Journal of Erosion Control Engineering*, 9(4), 174–178. <https://doi.org/10.13101/ijece.9.174>
- Bardera, R., Sor, S., & García-Magariño, A. (2020). Aerodynamics of Mars 2020 rover wind sensors. In G. Pezzella, & A. Viviani (Eds.), *Mars exploration (chapter 5)*. IntechOpen. <https://doi.org/10.5772/intechopen.90912>

Acknowledgments

LR was supported by the Dutch Research Council (NWO)—Grant OCENW. KLEIN.495 to TdH. The visits to the labs were funded by Europlanet—project number 20-EPN-015 to TdH, Europlanet—project number 20-EPN-023 to LR, and partly in-kind by the School of Physical Sciences of the Open University under the leadership of MRP through UK Space Agency Grant ST/X006549/1. We also acknowledge funding from the CNRS INSU Programme Nationale de Planétologie. SJC is grateful for financial support of the French Space Agency CNES for her HiRISE and CaSSIS work. Both the Mars Simulation Wind Tunnel laboratory and the Mars chamber of the HVI-lab at the Open University are members of Europlanet (2024) RI and have received funding from the European Union's Horizon 2020 research and innovation programme under grant agreement No 871149. The authors thank the spacecraft and instrument engineering teams for the successful completion and operation of CaSSIS. CaSSIS is a project of the University of Bern funded through the Swiss Space Office via ESA's PRODEX programme. The instrument hardware development was also supported by the Italian Space Agency (ASI) (ASI-INAF agreement no. I/018/12/0), INAF/Astronomical Observatory of Padova, and the Space Research Center (CBK) in Warsaw. Support from SGF (Budapest), the University of Arizona (LPL), and NASA are also gratefully acknowledged.

- Blair, T. C., & McPherson, J. G. (1998). Recent debris-flow processes and resultant form and facies of the Dolomite alluvial fan, Owens Valley, California. *Journal of Sedimentary Research*, 68(5), 800–818. <https://doi.org/10.2110/jsr.68.800>
- Cedillo-Flores, Y., Treiman, A. H., Lasue, J., & Clifford, S. M. (2011). CO₂ gas fluidization in the initiation and formation of Martian polar gullies. *Geophysical Research Letters*, 38(21), L21202. <https://doi.org/10.1029/2011GL049403>
- Conway, S. J., de Haas, T., & Harrison, T. N. (2019). Martian gullies: A comprehensive review of observations, mechanisms and insights from Earth analogues. *Geological Society, London, Special Publications*, 467(1), 7–66. <https://doi.org/10.1144/SP467.14>
- Conway, S. J., Lamb, M. P., Balme, M. R., Towner, M. C., & Murray, J. B. (2011). Enhanced runoff and erosion by overland flow at low pressure and sub-freezing conditions: Experiments and application to Mars. *Icarus*, 211(1), 443–457. <https://doi.org/10.1016/j.icarus.2010.08.026>
- Costard, F., Forget, F., Mangold, N., & Peulvast, J. P. (2002). Formation of recent Martian debris flows by melting of near-surface ground ice at high obliquity. *Science*, 295(5552), 110–113. <https://doi.org/10.1126/science.1066698>
- Cottin, H., Kotler, J. M., Bartik, K., Cleaves, H. J., Cockell, C. S., De Vera, J.-P. P., et al. (2017). Astrobiology and the possibility of life on Earth and elsewhere. *Space Science Reviews*, 209(1–4), 1–42. <https://doi.org/10.1007/s11214-015-0196-1>
- de Haas, T., Braat, L., Leuven, J. R., Lokhorst, I. R., & Kleinhans, M. G. (2015). Effects of debris flow composition on runoff, depositional mechanisms, and deposit morphology in laboratory experiments. *Journal of Geophysical Research: Earth Surface*, 120(9), 1949–1972. <https://doi.org/10.1002/2015jf003525>
- de Haas, T., Densmore, A., Stoffel, M., Suwa, H., Imaizumi, F., Ballesteros-Cánovas, J., & Wasklewicz, T. (2018). Avulsions and the spatio-temporal evolution of debris-flow fans. *Earth-Science Reviews*, 177, 53–75. <https://doi.org/10.1016/j.earscirev.2017.11.007>
- de Haas, T., Hauber, E., Conway, S., Van Steijn, H., Johnsson, A., & Kleinhans, M. (2015). Earth-like aqueous debris-flow activity on Mars at high orbital obliquity in the last million years. *Nature Communications*, 6(1), 1–6. <https://doi.org/10.1038/ncomms8543>
- de Haas, T., Kleinhans, M. G., Carbonneau, P. E., Rubensdotter, L., & Hauber, E. (2015). Surface morphology of fans in the high-Arctic periglacial environment of Svalbard: Controls and processes. *Earth-Science Reviews*, 146, 163–182. <https://doi.org/10.1016/j.earscirev.2015.04.004>
- de Haas, T., McArdell, B. W., Conway, S. J., McElwaine, J. N., Kleinhans, M. G., Salese, F., & Grindrod, P. M. (2019). Initiation and flow conditions of contemporary flows in Martian gullies. *Journal of Geophysical Research: Planets*, 124(8), 2246–2271. <https://doi.org/10.1029/2018JE005899>
- de Haas, T., & Woerkom, T. V. (2016). Bed scour by debris flows: Experimental investigation of effects of debris-flow composition. *Earth Surface Processes and Landforms*, 41(13), 1951–1966. <https://doi.org/10.1002/esp.3963>
- Dickson, J. L., Palumbo, A. M., Head, J. W., Kerber, L., Fassett, C. L., & Kreslavsky, M. A. (2023). Gullies on Mars could have formed by melting of water ice during periods of high obliquity. *Science*, 380(6652), 1363–1367. <https://doi.org/10.1126/science.abk2464>
- Diniega, S., Bramson, A. M., Buratti, B., Buhler, P., Burr, D. M., Chojnacki, M., et al. (2021). Modern Mars' geomorphological activity, driven by wind, frost, and gravity. *Geomorphology*, 380, 107627. <https://doi.org/10.1016/j.geomorph.2021.107627>
- Diniega, S., Byrne, S., Bridges, N. T., Dundas, C. M., & McEwen, A. S. (2010). Seasonality of present-day Martian dune-gully activity. *Geology*, 38(11), 1047–1050. <https://doi.org/10.1130/G31287.1>
- Diniega, S., Hansen, C., McElwaine, J., Hugenholtz, C., Dundas, C., McEwen, A., & Bourke, M. (2013). A new dry hypothesis for the formation of Martian linear gullies. *Icarus*, 225(1), 526–537. <https://doi.org/10.1016/j.icarus.2013.04.006>
- Dundas, C. M., Conway, S. J., & Cushing, G. E. (2022). Martian gully activity and the gully sediment transport system. *Icarus*, 386, 115133. <https://doi.org/10.1016/j.icarus.2022.115133>
- Dundas, C. M., Diniega, S., Hansen, C. J., Byrne, S., & McEwen, A. S. (2012). Seasonal activity and morphological changes in Martian gullies. *Icarus*, 220(1), 124–143. <https://doi.org/10.1016/j.icarus.2012.04.005>
- Dundas, C. M., Diniega, S., & McEwen, A. S. (2015). Long-term monitoring of Martian gully formation and evolution with MRO/HiRISE. *Icarus*, 251, 244–263. <https://doi.org/10.1016/j.icarus.2014.05.013>
- Dundas, C. M., McEwen, A. S., Diniega, S., Byrne, S., & Martínez-Alonso, S. (2010). New and recent gully activity on Mars as seen by HiRISE. *Geophysical Research Letters*, 37(7), L07202. <https://doi.org/10.1029/2009GL041351>
- Dundas, C. M., McEwen, A. S., Diniega, S., Hansen, C. J., Byrne, S., & McElwaine, J. N. (2017). The formation of gullies on Mars today. *Geological Society, London, Special Publications*, 467(1), 67–94. <https://doi.org/10.1144/SP467.5>
- Dundas, C. M., McEwen, A. S., Diniega, S., Hansen, C. J., Byrne, S., & McElwaine, J. N. (2019). scho. *Geological Society, London, Special Publications*, 467(1), 67–94. <https://doi.org/10.1144/SP467.5>
- Haberle, R. M., McKay, C. P., Schaeffer, J., Cabrol, N. A., Grin, E. A., Zent, A. P., & Quinn, R. (2001). On the possibility of liquid water on present-day Mars. *Journal of Geophysical Research*, 106(E10), 23317–23326. <https://doi.org/10.1029/2000JE001360>
- Hecht, M. H. (2002). Metastability of liquid water on Mars. *Icarus*, 156(2), 373–386. <https://doi.org/10.1006/icar.2001.6794>
- Hoffman, N. (2002). Active polar gullies on Mars and the role of carbon dioxide. *Astrobiology*, 2(3), 313–323. <https://doi.org/10.1089/153110702762027899>
- Holstein-Rathlou, C., Merrison, J., Iversen, J. J., Jakobsen, A. B., Nicolajsen, R., Nørnberg, P., et al. (2014). An environmental wind tunnel facility for testing meteorological sensor systems. *Journal of Atmospheric and Oceanic Technology*, 31(2), 447–457. <https://doi.org/10.1175/JTECH-D-13-00141.1>
- Hubert, J. F., & Filipov, A. J. (1989). Debris-flow deposits in alluvial fans on the west flank of the White Mountains, Owens Valley, California, U. S.A. *Sedimentary Geology*, 61(3), 177–205. [https://doi.org/10.1016/0037-0738\(89\)90057-2](https://doi.org/10.1016/0037-0738(89)90057-2)
- Hugenholtz, C. H. (2008). Frosted granular flow: A new hypothesis for mass wasting in Martian gullies. *Icarus*, 197(1), 65–72. <https://doi.org/10.1016/j.icarus.2008.04.010>
- Iverson, R. M. (1997). The physics of debris flows. *Reviews of Geophysics*, 35(3), 245–296. <https://doi.org/10.1029/97rg00426>
- Iverson, R. M. (2015). Scaling and design of landslide and debris-flow experiments. *Geomorphology*, 244, 9–20. <https://doi.org/10.1016/j.geomorph.2015.02.033>
- Iverson, R. M., & Denlinger, R. P. (2001). Flow of variably fluidized granular masses across three-dimensional terrain: I. Coulomb mixture theory. *Journal of Geophysical Research*, 106(B1), 537–552. <https://doi.org/10.1029/2000jb900329>
- Iverson, R. M., Logan, M., LaHusen, R. G., & Berti, M. (2010). The perfect debris flow? Aggregated results from 28 large-scale experiments. *Journal of Geophysical Research*, 115(F3), F03005. <https://doi.org/10.1029/2009JF001514>
- Jessop, D., Kelfoun, K., Labazuy, P., Mangeny, A., Roche, O., Tillier, J.-L., et al. (2012). Lidar derived morphology of the 1993 lascar pyroclastic flow deposits, and implication for flow dynamics and rheology. *Journal of Volcanology and Geothermal Research*, 245–246, 81–97. <https://doi.org/10.1016/j.jvolgeores.2012.06.030>
- Johnson, C. G., Kokelaar, B. P., Iverson, R. M., Logan, M., LaHusen, R. G., & Gray, J. M. N. T. (2012). Grain-size segregation and levee formation in geophysical mass flows. *Journal of Geophysical Research*, 117(F1), F01032. <https://doi.org/10.1029/2011JF002185>

- Johnsson, A., Reiss, D., Hauber, E., Hiesinger, H., & Zanetti, M. (2014). Evidence for very recent melt-water and debris flow activity in gullies in a young mid-latitude crater on Mars. *Icarus*, 235, 37–54. <https://doi.org/10.1016/j.icarus.2014.03.005>
- Khuller, A. R., Christensen, P. R., Harrison, T. N., & Diniega, S. (2021). The distribution of frosts on Mars: Links to present-day gully activity. *Journal of Geophysical Research: Planets*, 126(3), e2020JE006577. <https://doi.org/10.1029/2020JE006577>
- Kieffer, H. H. (2007). Cold jets in the Martian polar caps. *Journal of Geophysical Research*, 112(E8), E08005. <https://doi.org/10.1029/2006JE002816>
- Knauth, L., & Burt, D. M. (2002). Eutectic brines on Mars: Origin and possible relation to young seepage features. *Icarus*, 158(1), 267–271. <https://doi.org/10.1006/icar.2002.6866>
- Lanza, N., Meyer, G., Okubo, C., Newsom, H., & Wiens, R. (2010). Evidence for debris flow gully formation initiated by shallow subsurface water on Mars. *Icarus*, 205(1), 103–112. <https://doi.org/10.1016/j.icarus.2009.04.014>
- Levy, J., Head, J., Dickson, J., Fassett, C., Morgan, G., & Schon, S. (2010). Identification of gully debris flow deposits in Protonilus Mensae, Mars: Characterization of a water-bearing, energetic gully-forming process. *Earth and Planetary Science Letters*, 294(3), 368–377. <https://doi.org/10.1016/j.epsl.2009.08.002>
- Lube, G., Cronin, S. J., Platz, T., Freundt, A., Procter, J. N., Henderson, C., & Sheridan, M. F. (2007). Flow and deposition of pyroclastic granular flows: A type example from the 1975 Ngauruhoe eruption, New Zealand. *Journal of Volcanology and Geothermal Research*, 161(3), 165–186. <https://doi.org/10.1016/j.jvolgeores.2006.12.003>
- Malin, M. C., & Edgett, K. S. (2000). Evidence for recent groundwater seepage and surface runoff on Mars. *Science*, 288(5475), 2330–2335. <https://doi.org/10.1126/science.288.5475.2330>
- Martinez, G. M., Newman, C., De Vicente-Retortillo, A., Fischer, E., Renno, N., Richardson, M., et al. (2017). The modern near-surface Martian climate: A review of in-situ meteorological data from Viking to Curiosity. *Space Science Reviews*, 212(1–2), 295–338. <https://doi.org/10.1007/s11214-017-0360-x>
- Parsons, J. D., Whipple, K. X., & Simoni, A. (2001). Experimental study of the grain-flow, fluid-mud transition in debris flows. *The Journal of Geology*, 109(4), 427–447. <https://doi.org/10.1086/320798>
- Pasquon, K., Conway, S., Vincendon, M., Massé, M., Raack, J., Noblet, A., et al. (2023). Insights into the interaction between defrosting seasonal ices and gully activity from CaSSIS and HiRISE observations in Sisyphi Cavi, Mars. *Planetary and Space Science*, 235, 105743. <https://doi.org/10.1016/j.pss.2023.105743>
- Pasquon, K., Gargani, J., Massé, M., Vincendon, M., Conway, S. J., Séjourné, A., et al. (2019). Present-day development of gully-channel sinuosity by carbon dioxide gas supported flows on Mars. *Icarus*, 329, 296–313. <https://doi.org/10.1016/j.icarus.2019.03.034>
- Pilorget, C., & Forget, F. (2016). Formation of gullies on Mars by debris flows triggered by CO₂ sublimation. *Nature Geoscience*, 9(1), 65–69. <https://doi.org/10.1038/ngeo2619>
- Raack, J., Conway, S. J., Heyer, T., Bickel, V. T., Philippe, M., Hiesinger, H., et al. (2020). Present-day gully activity in Sisyphi Cavi, Mars—Flow-like features and block movements. *Icarus*, 350, 113899. <https://doi.org/10.1016/j.icarus.2020.113899>
- Raack, J., Reiss, D., Appéré, T., Vincendon, M., Ruesch, O., & Hiesinger, H. (2015). Present-day seasonal gully activity in a south polar pit (Sisyphi Cavi) on Mars. *Icarus*, 251, 226–243. <https://doi.org/10.1016/j.icarus.2014.03.040>
- Richardson, M. I., & Mischna, M. A. (2005). Long-term evolution of transient liquid water on Mars. *Journal of Geophysical Research*, 110(E3), E03003. <https://doi.org/10.1029/2004JE002367>
- Roelofs, L., Colucci, P., & Haas, T. D. (2022). How debris-flow composition affects bed erosion quantity and mechanisms—An experimental assessment. *Earth Surface Processes and Landforms*, 47(8), 2151–2169. <https://doi.org/10.1002/esp.5369>
- Roelofs, L., Conway, S., van Dam, B., Merrison, J., Iversen, J., Sylvest, M., et al. (2024). *Data supplement to “The dynamics of CO₂-driven granular flows in gullies on Mars” (Technical Report)*. Utrecht University. <https://doi.org/10.24416/UU01-WXXMZf>
- Roelofs, L., Conway, S. J., de Haas, T., Dundas, C., Lewis, S. R., McElwaine, J., et al. (2024). How, when and where current mass flows in Martian gullies are driven by CO₂ sublimation. *Communications Earth & Environment*, 5(1), 125. <https://doi.org/10.1038/s43247-024-01298-7>
- Roelofs, L., Nota, E. W., Flipsen, T. C. W., Colucci, P., & de Haas, T. (2023). How bed composition affects erosion by debris flows—An experimental assessment. *Geophysical Research Letters*, 50(14), e2023GL103294. <https://doi.org/10.1029/2023GL103294>
- Rothery, D. A., Massironi, M., Alemanno, G., Barraud, O., Besse, S., Bott, N., et al. (2020). Rationale for BepiColombo studies of Mercury’s surface and composition. *Space Science Reviews*, 216(4), 1–46. <https://doi.org/10.1007/s11214-020-00694-7>
- Rowley, P. D., Kuntz, M. A., & Macleod, N. S. (1981). Pyroclastic-flow deposits. In *The 1980 eruptions of Mount St. Helens, Washington* (pp. 489–512). USGS. <https://doi.org/10.3133/pp1250>
- Scully, J. E., Russell, C. T., Yin, A., Jaumann, R., Carey, E., Castillo-Rogez, J., et al. (2015). Geomorphological evidence for transient water flow on Vesta. *Earth and Planetary Science Letters*, 411, 151–163. <https://doi.org/10.1016/j.epsl.2014.12.004>
- Shakeel, H., Wei, H., & Pomeroy, J. (2018). Measurements of enthalpy of sublimation of Ne, N₂, O₂, Ar, CO₂, Kr, Xe, and H₂O using a double paddle oscillator. *The Journal of Chemical Thermodynamics*, 118, 127–138. <https://doi.org/10.1016/j.jct.2017.11.004>
- Sinha, R. K., & Ray, D. (2023). Morphological changes currently occurring in sand-filled gully channels on Mars: Implications for the role of substrates inside channels. *Icarus*, 390, 115334. <https://doi.org/10.1016/j.icarus.2022.115334>
- Sinha, R. K., Vijayan, S., Shukla, A. D., Das, P., & Bhattacharya, F. (2018). Gullies and debris-flows in Ladakh Himalaya, India: A potential Martian analogue. *Geological Society, London, Special Publications*, 467(1), 315–342. <https://doi.org/10.1144/SP467.9>
- Smith, G., Rowley, P., Williams, R., Giordano, G., Trolese, M., Silleni, A., et al. (2020). A bedform phase diagram for dense granular currents. *Nature Communications*, 11(1), 2873. <https://doi.org/10.1038/s41467-020-16657-z>
- Stephenson, R. M. (1987). *Handbook of the thermodynamics of organic compounds*. Elsevier. <https://doi.org/10.1007/978-94-009-3173-2>
- Stock, J. D., & Dietrich, W. E. (2003). Valley incision by debris flows: Evidence of a topographic signature. *Water Resources Research*, 39(4), 1089. <https://doi.org/10.1029/2001WR001057>
- Sylvest, M. E., Conway, S. J., Patel, M. R., Dixon, J. C., & Barnes, A. (2016). Mass wasting triggered by seasonal CO₂ sublimation under Martian atmospheric conditions: Laboratory experiments. *Geophysical Research Letters*, 43(24), 12363–12370. <https://doi.org/10.1002/2016GL071022>
- Sylvest, M. E., Dixon, J. C., Conway, S. J., Patel, M. R., McElwaine, J. N., Hagermann, A., & Barnes, A. (2019). CO₂ sublimation in Martian gullies: Laboratory experiments at varied slope angle and regolith grain sizes. *Geological Society, London, Special Publications*, 467(1), 343–371. <https://doi.org/10.1144/SP467.11>
- Zhou, G. G., Li, S., Song, D., Choi, C. E., & Chen, X. (2019). Depositional mechanisms and morphology of debris flow: Physical modelling. *Landslides*, 16(2), 315–332. <https://doi.org/10.1007/s10346-018-1095-9>